**SANDIA REPORT**
SAND2012-10109
Unlimited Release
Printed December 2012

# Structural Health and Prognostics Management for Offshore Wind Turbines: An Initial Roadmap

D. Todd Griffith, Nathanael C. Yoder, Brian R. Resor, Jonathan R. White, and Joshua A. Paquette

Prepared by
Sandia National Laboratories
Albuquerque, New Mexico 87185 and Livermore, California 94550

Sandia National Laboratories is a multi-program laboratory managed and operated by Sandia Corporation, a wholly owned subsidiary of Lockheed Martin Corporation, for the U.S. Department of Energy's National Nuclear Security Administration under contract DE-AC04-94AL85000.



Issued by Sandia National Laboratories, operated for the United States Department of Energy by Sandia Corporation.



Available to DOE and DOE contractors from
U.S. Department of Energy
Office of Scientific and Technical Information
P.O. Box 62
Oak Ridge, TN 37831

Telephone: (865) 576-8401
Facsimile: (865) 576-5728
E-Mail: reports@adonis.osti.gov
Online ordering: http://www.osti.gov/bridge

Available to the public from
U.S. Department of Commerce
National Technical Information Service
5285 Port Royal Rd.
Springfield, VA 22161

Telephone: (800) 553-6847
Facsimile: (703) 605-6900
E-Mail: orders@ntis.fedworld.gov
Online order: http://www.ntis.gov/help/ordermethods.asp?loc=7-4-0#online

SAND2012-10109
Unlimited Release
Printed December 2012

# Structural Health and Prognostics Management for Offshore Wind Turbines: An Initial Roadmap

D. Todd Griffith, Brian R. Resor, Jonathan R. White, Joshua A. Paquette
Wind Energy Technology Department
Sandia National Laboratories
P.O. Box 5800
Albuquerque, New Mexico 87185-MS1124

Nathanael C. Yoder
ATA Engineering
11995 El Camino Real, Suite 200
San Diego, CA 92130

**Abstract**

Operations and maintenance costs for offshore wind plants are expected to be significantly higher than the current costs for onshore plants. One way in which these costs may be able to be reduced is through the use of a structural health and prognostic management system as part of a condition based maintenance paradigm with smart load management. To facilitate the creation of such a system a multiscale modeling approach has been developed to identify how the underlying physics of the system are affected by the presence of damage and how these changes manifest themselves in the operational response of a full turbine. The developed methodology was used to investigate the effects of a candidate blade damage feature, a trailing edge disbond, on a 5-MW offshore wind turbine and the measurements that demonstrated the highest sensitivity to the damage were the local pitching moments around the disbond. The multiscale method demonstrated that these changes were caused by a local decrease in the blade's torsional stiffness due to the disbond, which also resulted in changes in the blade's local strain field. Full turbine simulations were also used to demonstrate that derating the turbine power by as little as 5% could extend the fatigue life of a blade by as much as a factor of 3. The integration of the health monitoring information, conceptual repair cost versus damage size information, and this load management methodology provides an *initial roadmap* for reducing operations and maintenance costs for offshore wind farms while increasing turbine availability and overall profit.

# CONTENTS

# FIGURES

# TABLES

## NOMENCLATURE

| | |
|---|---|
| BPE | Beam Property Extraction |
| CBM | condition based maintenance |
| FE | finite element |
| kWh | kilowatt-hour |
| LP | low pressure |
| MW | Megawatt |
| NREL | National Renewable Energy Laboratory |
| NuMAD | Numerical Manufacturing and Design Tool |
| O&M | operations and maintenance |
| RMS | root mean square |
| SHPM | structural health and prognostics management |
| SNL | Sandia National Laboratories |
| TE | trailing edge |
| UD | uni-directional |

# EXECUTIVE SUMMARY

Offshore wind energy could potentially play a significant role in helping the U.S. obtain an energy portfolio composed of clean, renewable and diversified resources. One current obstacle to the utilization of offshore wind energy is that most projections put the operations and maintenance (O&M) costs of offshore wind farms between 2 to 5 times the current average O&M costs for onshore wind farms [1]. One way in which those costs may be reduced is through a simple yet effective structural health monitoring system as part of an overall condition based maintenance paradigm. A successful health monitoring system would be able to reduce or eliminate unplanned or unnecessary maintenance as well as reducing logistic lead times and optimizing supply chain management through the use of prognostics (predictive estimates of damage).

**A methodology has been created to aid in the development and optimization of a structural health and prognostics management (SHPM) system for wind turbine blades using physics-based simulations.** The developed scheme is a multiscale modeling and simulation approach that propagates the effects of damage from high fidelity local simulations to full turbine simulations using reduced order models as illustrated in Figure 1. This technique can be used as an initial roadmap for the development of future health monitoring systems because it allows for the investigation of the effects of damage on both local and global scales. Globally, the operational responses of the full turbine models can be analyzed for the development of health monitoring algorithms and identification of the optimal measurement types, locations, and directions. The loads from these full turbine simulations can then be applied to high fidelity models in order to investigate the localized effects of damage.

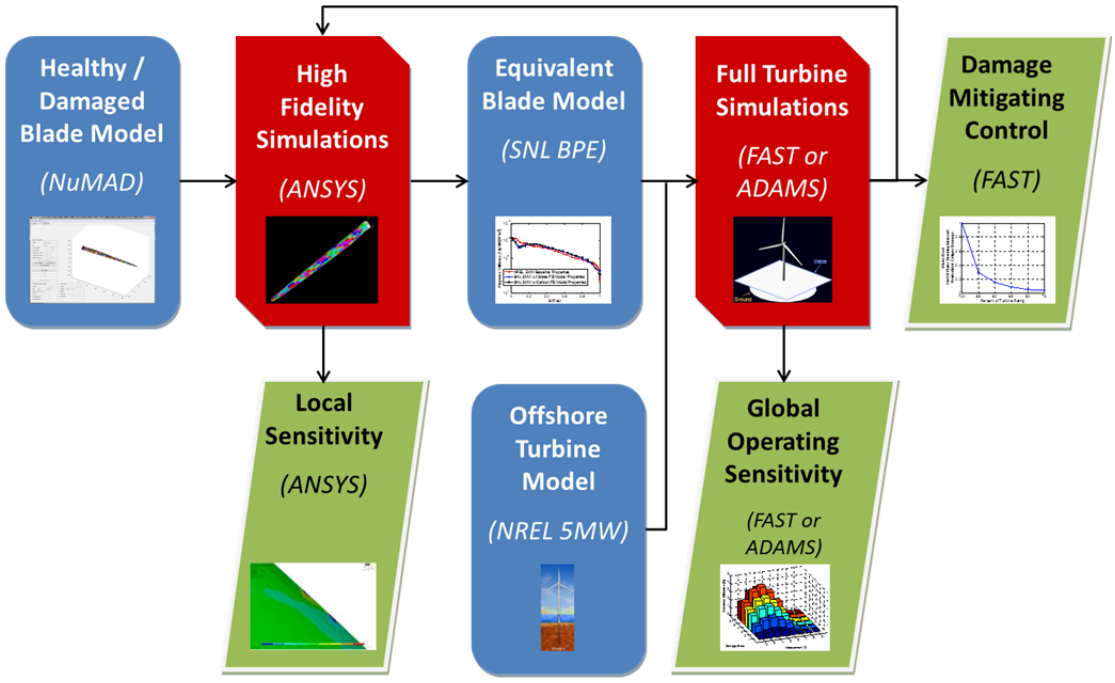


**Figure 1. The multiscale modeling and simulation methodology designed to aid in the development and optimization of health monitoring systems for wind turbine blades.**

As a representative example of how the developed methodology could be used to evaluate health monitoring systems, the effects of a trailing edge (TE) disbond on a 5-MW offshore wind turbine were investigated. Local analyses indicated that the TE disbond resulted in a local decrease in the torsional stiffness and change in strain field of the blade around the disbond, as shown by certain mode shapes such as the one in Figure 2. In global simulations (full turbine), the damage was most apparent in the sensitivity of the local per-revolution pitching moment of the damage blade around the disbond location (Figure 3). **The simulation results, clearly illustrated the benefit of the multiscale modeling approach and the utility of local strain measurements around the damage location for detection of TE disbonds.**

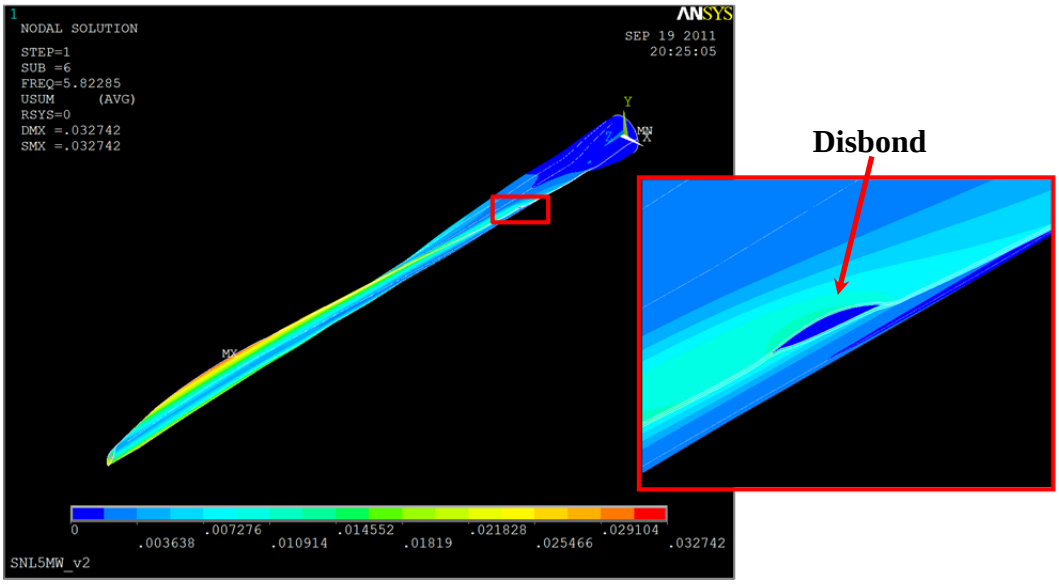


**Figure 2. The TE separation in the first torsional mode shape of a damaged blade.**

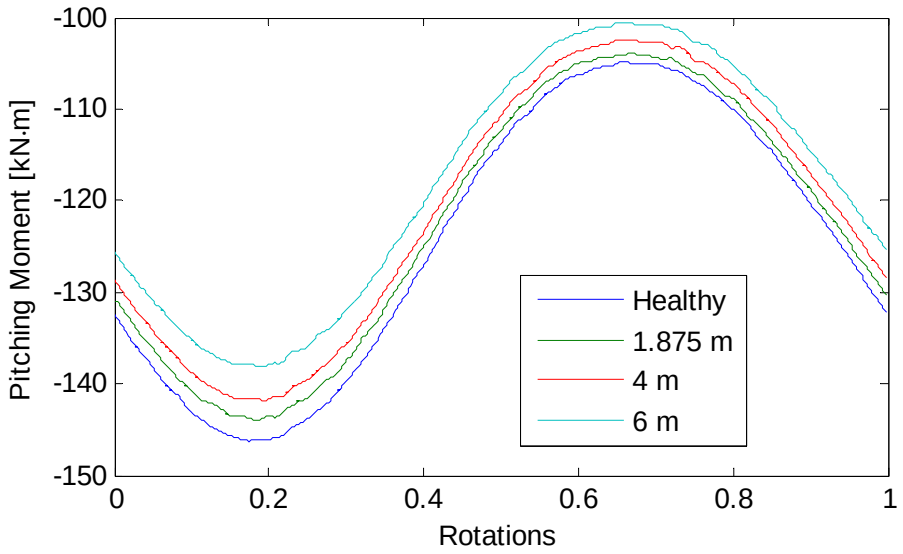


**Figure 3. The increase in the once per-revolution local pitching moment of the healthy blade and blades with a disbond that was 1.875, 4 or 6 meters in length.**

In addition to significant improvement in O&M costs of wind turbines, a structural health and prognostics monitoring system can be used as an integral component of health-driven wind turbine control. Consequently, damage mitigating control methodologies were investigated for smart turbine load management. **These initial simulations found that derating a turbine power production by as little as 5% resulted in a reduction in the equivalent loading by 10% and a blade fatigue life extension of 300%, as shown in Figure 4.** Therefore, if the health of a turbine is known, the power production of that turbine could be derated slightly to avoid costly unscheduled repairs and coordinate the lower-cost scheduled repair of many turbines. While further research into the optimal damage mitigating control methodologies is needed, it is evident that significant extensions of life can be achieved through small and simple changes in the turbine's operation. Furthermore, these load management strategies could prove especially beneficial for offshore turbines where maintenance may be limited by the weather and the increased possibility of servicing multiple turbines during a single visit to the wind plant may result in significantly reduced offshore O&M costs.

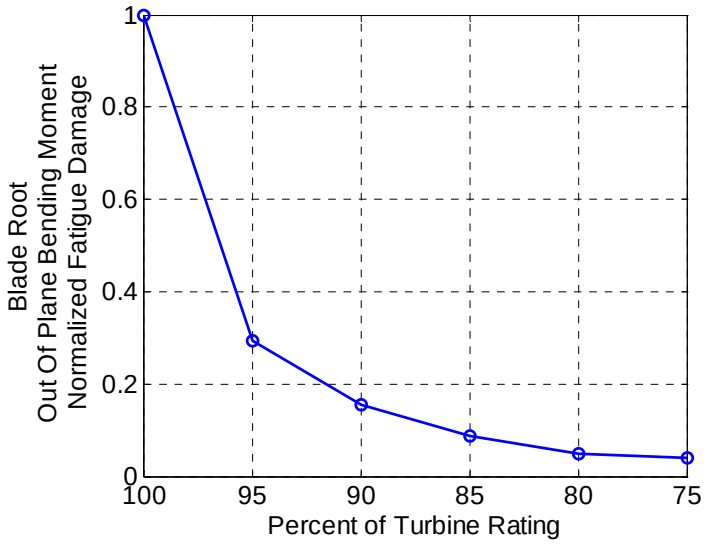


**Figure 4. Normalized fatigue damage due as a function of turbine rating.**

# 1. INTRODUCTION

Offshore wind energy in the United States is an untapped energy resource that could play a pivotal role in helping the U.S. obtain an energy portfolio composed of clean, renewable and diversified resources. Some of the drivers for the utilization of offshore wind include the proximity of the offshore resources to population centers and the potential for higher capacity factors due to higher resource winds [1, 2]. Because of these and other potential benefits of offshore wind, the Offshore Wind Innovation and Demonstration initiative has developed an ambitious goal of deploying 10 GW of offshore capacity by 2020 at a cost of energy of only $0.10/ kWh [3].

## 1.1. Drivers for Offshore SHPM

As of June 2011, while nine offshore projects totaling over 2 GW of capacity were in various stages of the permitting and development process, no offshore wind energy projects had been installed in the United States [4]. Part of the reason for this lack of development is that operations and maintenance (O&M) costs are expected to be significantly higher for offshore wind turbines than onshore wind turbines. Recent projections of O&M costs have ranged between $11 and $66 U.S. dollars per megawatt-hour with the majority of estimates being between 2 to 5 times the cost of onshore O&M [1]. These higher O&M costs represent a larger overall proportion of the cost of energy than for onshore turbines even when the large initial investment required for the installation of offshore turbines is included [5]. One of the reasons that O&M costs are likely to be higher offshore than onshore is that the offshore environment will bring with it increased loading which is relatively uncharacterized due to the lack of existing offshore installations. Offshore turbines will also have to be built to withstand the environmental harshness of the offshore environment. Lastly, access to the turbines will be difficult, costly, and occasionally may not be possible due to high sea states [1,6].

## 1.2. SHPM Benefits

One potential way in which these higher O&M costs could be addressed is through the use of a structural health and prognostics management (SHPM) system as part of a condition based maintenance (CBM) paradigm [6-12]. By continuously monitoring the health, or condition, of structural components in each wind turbine from land, required maintenance actions can be scheduled ahead of time and performed when they are needed rather than on a preset schedule or only after failure has already occurred. The benefits of a CBM strategy are expected to include less regular maintenance, the reduction or avoidance of unscheduled maintenance and improved supply chain management [6, 9-11].

Furthermore, because wind turbines are active systems, monitoring the health of wind turbine components allows turbines to be operated based on their health so that smart turbine load management strategies can be used to optimize the profit of the entire wind plant. For example, if a turbine blade becomes damaged and that damage is detected at an early stage by the SHPM system, the turbine could be derated so that smaller less costly repairs could be performed on the turbine. While this action would reduce the amount of power generated by the turbine in the

short-term, it may allow for less extensive maintenance actions to be performed, extend the overall life of the turbine, and allow for multiple turbines to be serviced during the same visit to the plant in order to maximize the overall profit of the wind power plant. In addition, the SHPM system could provide information to avoid catastrophic failures by alerting operators to the presence of damage before it reaches dangerous levels.

# 2. MULTISCALE SIMULATION APPROACH

To facilitate the investigation of SHPM systems for wind turbine blades using operational responses, a multiscale modeling approach was developed that propagates the effects of damage from high fidelity local simulations to full turbine simulations using reduced order models. A simulation campaign was then performed to identify operational response measurements that are sensitive to a representative form of damage. These simulations were an essential first step in identifying promising measurements for use in the operational monitoring of offshore wind turbines because of the scarcity of data from offshore wind turbines. In addition, simulations provide the unique ability to cost effectively investigate the sensitivity of many different potential measurements and measurement locations along with many types of blade or turbine damage while eliminating variability from sources other than damage.

In order to accurately capture the effects of damage on an offshore wind turbine's response a multiscale modeling approach was used. The simulation approach used high fidelity blade and damage models to model the influence of damage on the blade. This model was then reduced to an equivalent blade model of sufficient resolution to capture the influence of the damage while still being able to be integrated into simulations of a full offshore wind turbine. In addition to the analysis of the results from these full turbine simulations, the equivalent loads from these simulations can be fed back into the high fidelity model so that localized sensitivity measures can be obtained. The overall approach is shown in flowchart form in Figure 5. As an extension of this work even more accurate and refined damage modeling methodologies could be used to create the damage blade models or model the propagation of damage.

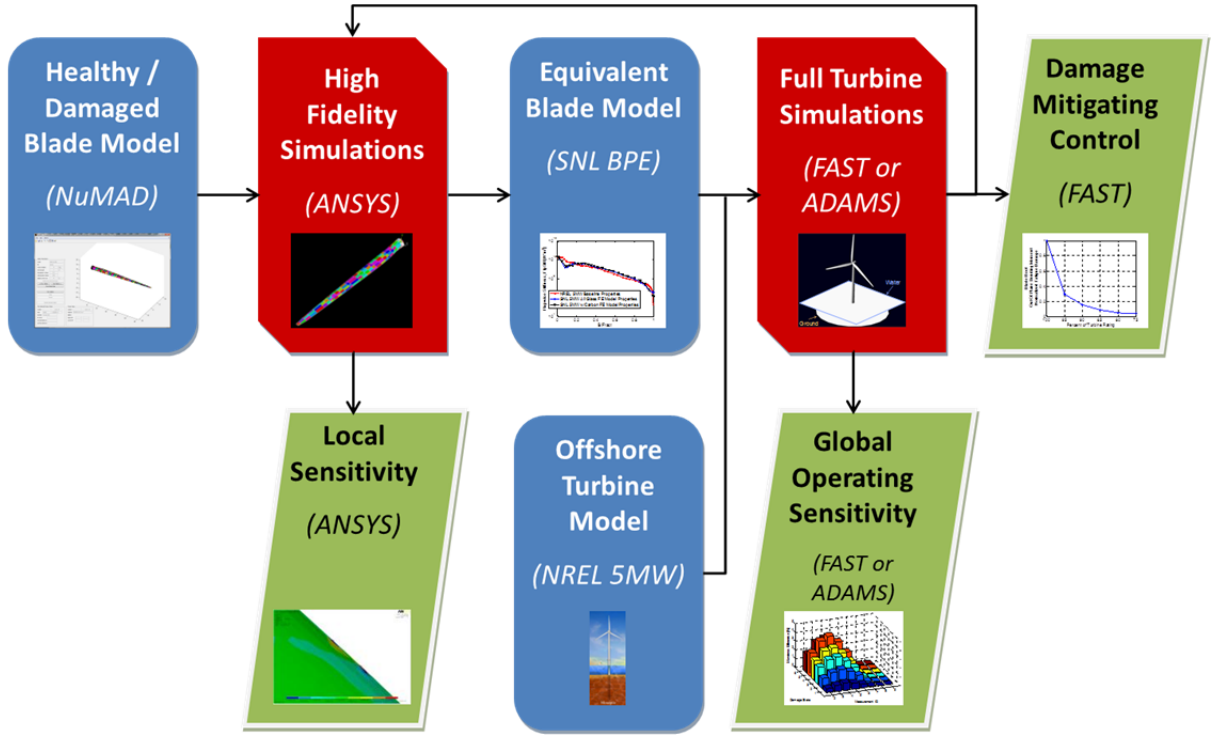


**Figure 5. Developed simulation methodology for the identification of operational response measurements that are the most sensitive to damage.**

In order to perform the desired simulations a variety of different software packages had to be integrated. The software packages that were used to obtain the results in this report are indicated in parenthesis in the Figure 5 flowchart. Sandia National Laboratories' (SNL's) Numerical Manufacturing and Design Tool (NuMAD) software was used to create a high fidelity blade model in the commercial finite element software package ANSYS. A trailing edge (TE) disbond damage feature was then introduced into the model and equivalent beam properties were extracted using SNL's Beam Property Extraction (BPE) software. The reduced order models were then integrated into a full turbine model for simulations of the damaged turbine in either FAST [13] or MSC.ADAMS [14]. Results from each stage of this modeling process were then used to assess the influence of the damage on the response of the blade and the turbine as a whole and determine a subset of measurements that could prove beneficial for future SHPM investigations. Global operating sensitivity to damage was calculated using either the FAST or MSC.ADAMS turbine simulations. Aerodynamic loads from the full turbine simulations were fed back to the high fidelity simulation to quantify the localized damage sensitivity.

Even if a SHPM system proves effective in detecting damage, in order to utilize the information most effectively, the cost of repairing the damage should be taken into account in the CBM framework. This allows the health information to not just be used for the scheduling and optimization of the maintenance procedures, but to also be used to optimize the operation of the slightly damaged turbines. By propagating aerodynamic loads from full turbine simulations back into local high fidelity simulations it was demonstrated that significant extensions in the fatigue life of a blade could be achieved by derating a turbine's power production by as little as 5%. Therefore, using smart turbine load management strategies with damage mitigating control could allow for the productive life of blades to be extended while slowing the propagation of damage until the appropriate maintenance can be performed in the most cost effective manner.

This report will attempt to address the integration of SHPM into the O&M process for wind power plants in several ways. First a multiscale simulation based methodology that can be used to determine the measurement channels that are the most sensitive to a representative form of damage in a cost-effective manner has been developed and can be extended to investigate the application of other potential health monitoring methods. Secondly, the dependence of repair costs on damage size has been recognized through illustration of a conceptual model. The utility of integrating the knowledge of these costs with damage state of the turbine can be utilized not just to perform more cost-effective CBM but also to operate individual turbines to extend their life and maximize overall plant profit.

# 3. FIVE MEGAWATT OFFSHORE TURBINE MODEL DEVELOPMENT

In order to investigate the potential of using operational measurements for the SHPM of offshore wind turbines a model of a representative offshore turbine was needed. This section will describe the overall turbine model that was used in this simulation study and then move on to detail the development of the high fidelity wind turbine blade model. Next, the damage modeling methodology used in this study and the development of reduced order blade models from the finite element models will be discussed.

## 3.1. Five Megawatt Turbine Model Description

A representative utility-scale multimegawatt turbine model known as the National Renewable Energy Laboratory (NREL) offshore 5-MW baseline wind turbine was developed by NREL in order to support concept studies aimed at assessing offshore wind technology [15]. The model is used as a reference by research teams throughout the world to standardize baseline offshore wind turbine specifications and to quantify the benefits of advanced land- and sea-based wind energy technologies. The wind turbine is a conventional three-bladed upwind variable-speed variable blade-pitch-to-feather-controlled turbine. The model was created using broad design information from published documents of turbine manufacturers, with a heavy emphasis on the REpower 5-MW machine. Detailed data was unavailable so publicly available properties from the conceptual models in the WindPACT, RECOFF, and DOWEC projects were used to create the 5-MW model. The specifications of the NREL offshore 5-MW baseline wind turbine include aerodynamic, structural, and control-system properties. Table 1 lists the basic specifications of the 5-MW turbine model and an image of the MSC.ADAMS model of the offshore wind turbine is shown in Figure 6.

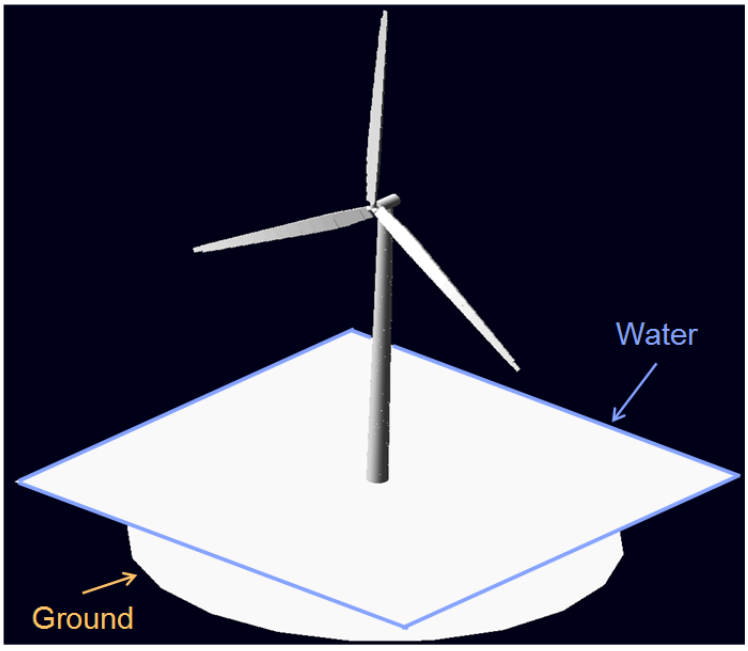


**Figure 6. An image of the offshore 5-MW wind turbine model in MSC.ADAMS.**

**Table 1. Gross properties of the NREL 5-MW baseline wind turbine.**

| Property | Value |
|---|---|
| Rating | 5 MW |
| Rotor Orientation, Configuration | Upwind, 3 Blades |
| Control | Variable Speed, Collective Pitch |
| Drivetrain | High Speed, Multiple-Stage Gearbox |
| Rotor, Hub Diameter | 126 m, 3 m |
| Hub Height | 90 m |
| Cut-In, Rated, Cut-Out Wind Speed | 3 m/s, 11.4 m/s, 25 m/s |
| Cut-In, Rated Rotor Speed | 6.9 rpm, 12.1 rpm |
| Rated Tip Speed | 80 m/s |
| Overhang, Shaft Tilt, Precone | 5 m, 5º, 2.5º |
| Rotor Mass | 110,000 kg |
| Nacelle Mass | 240,000 kg |
| Tower Mass | 347,460 kg |
| Water Depth | 20 m |
| Wave Model | JONSWAP/Pierson-Moskowitz Spectrum |
| Significant Wave Height | 6 m |
| Platform | Fixed-Bottom Monopile |

To obtain a blade model that could be used as part of full turbine simulations, Sandia's NuMAD software was used to design a detailed composite layup. NuMAD allowed complex blade models to be integrated with damage models in ANSYS after which the effective beam properties of the damaged blade could be obtained using the SNL BPE software. The following sections detail the development of the 5-MW blade model and the damage modeling methodology used to model a TE disbond.

## 3.2. Five Megawatt Blade Model Development

The publicly available NREL 5-MW turbine aeroelastic model and associated report do not contain detailed information about the blade design, i.e. material selection and material placement, airfoil shapes and shear webs. The publicly available model only contains a desired distribution of effective cross sectional properties for a blade. However, a detailed computer model of the blade is needed in order to perform analyses to support structural health monitoring research on a system of this size. Sandia's NuMAD software was used to create the detailed blade model for the current work. NuMAD is a preprocessor for ANSYS, a commercially available finite element (FE) analysis software package. NuMAD translates material properties, material locations, airfoil shapes and shear web locations into a large degree-of-freedom ANSYS FE model composed of shell elements. ANSYS is used to solve the model's response to input forces that are representative of aerodynamic loads on the blade. Calculation of localized strains, blade panel buckling response and general blade deformation are all important analyses that can be performed in ANSYS.

The blade model developed for this work used existing blade geometry data from the DOWEC study and composite layup information from the UpWind program in a preliminary 5-MW

baseline blade model. The preliminary all-glass composite layup (a modified version of UpWind) produced a blade that is too heavy compared to the blade weight specified for the 5-MW turbine in the NREL report [15]. Weight reduction of the initial blade was achieved through the use of carbon fiber spar caps, which at the same time enabled preservation of the specified distribution of blade stiffness. Material properties for uni-directional (UD) carbon fiber (Newport 307) were obtained from the Sandia-MSU Materials Database [16] and used for the carbon spar caps. Figure 7 illustrates the distribution of material layers along the span of the blade.

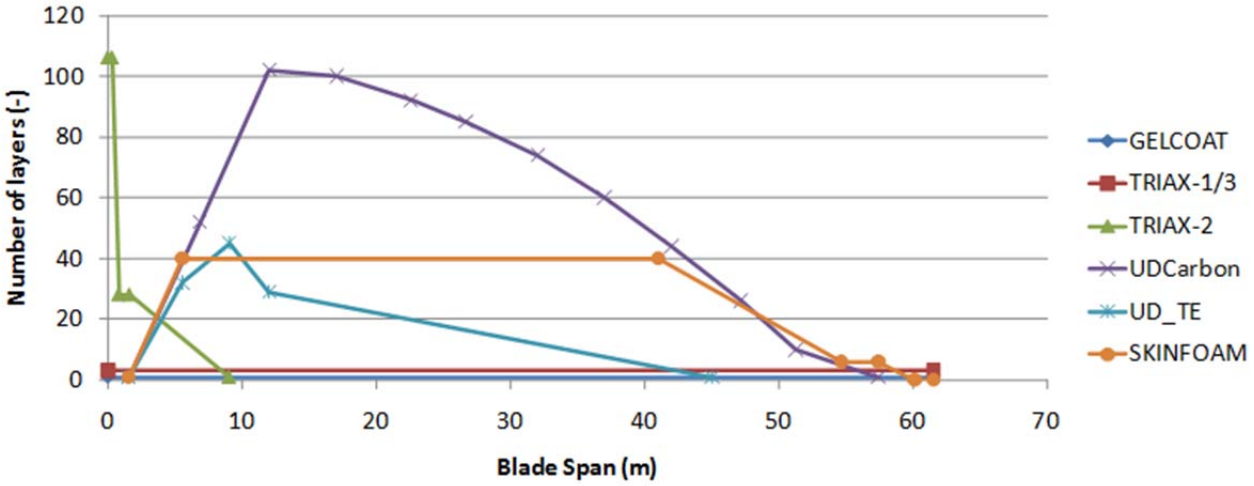


**Figure 7. Distribution of layers along the span of the blade model.**

The TU-Delft family of airfoils was used for the majority of this blade. NACA 64-series airfoils were used in the final one-third blade span. No transition airfoils were reported between the root circle and airfoil at maximum chord. Intermediate airfoil shapes were developed as part of this work using a technique that preserves the blending of camber lines while also preserving a smooth blade thickness profile. Figure 8 shows a picture of the completed finite element model in ANSYS.

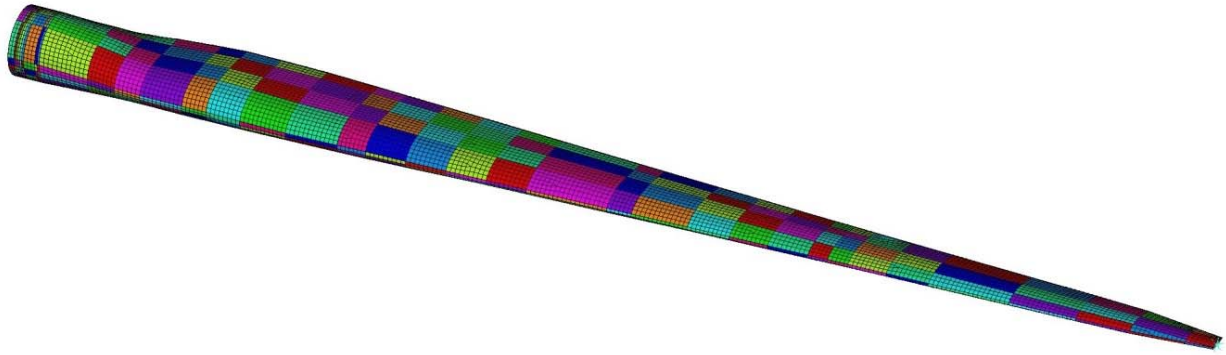

**Figure 8. Overview of the ANSYS finite element mesh for the 5-MW blade model.**

The Sandia Beam Property Extraction (BPE) tool was used to determine the equivalent beam property distributions for this blade model. The BPE tool is discussed in more detail in Section

3.3 of this report. Figure 9 shows three different curves representing beam properties: first, the specified properties taken directly from the NREL 5-MW aeroelastic system model, second, the properties computed using the preliminary all-glass blade model, and third, the properties computed using the blade model with carbon fiber spar caps. Figure 9 (a) shows the discrepancy between the NREL 5-MW specified mass distribution and the mass distribution achieved using fiberglass alone. It also shows the greatly decreased mass distribution achieved by replacing the fiberglass spar cap with the appropriate number of layers of unidirectional carbon fiber. The three remaining plots in Figure 9 ((b)-(d)) show the variations in the blade's stiffness parameters along the span of the blade while Table 2 shows the computed blade mass for each of the three scenarios. The inclusion of the carbon spar cap in the SNL 5MW blade resulted in good agreement with the mass and stiffness properties of the NREL 5MW baseline.

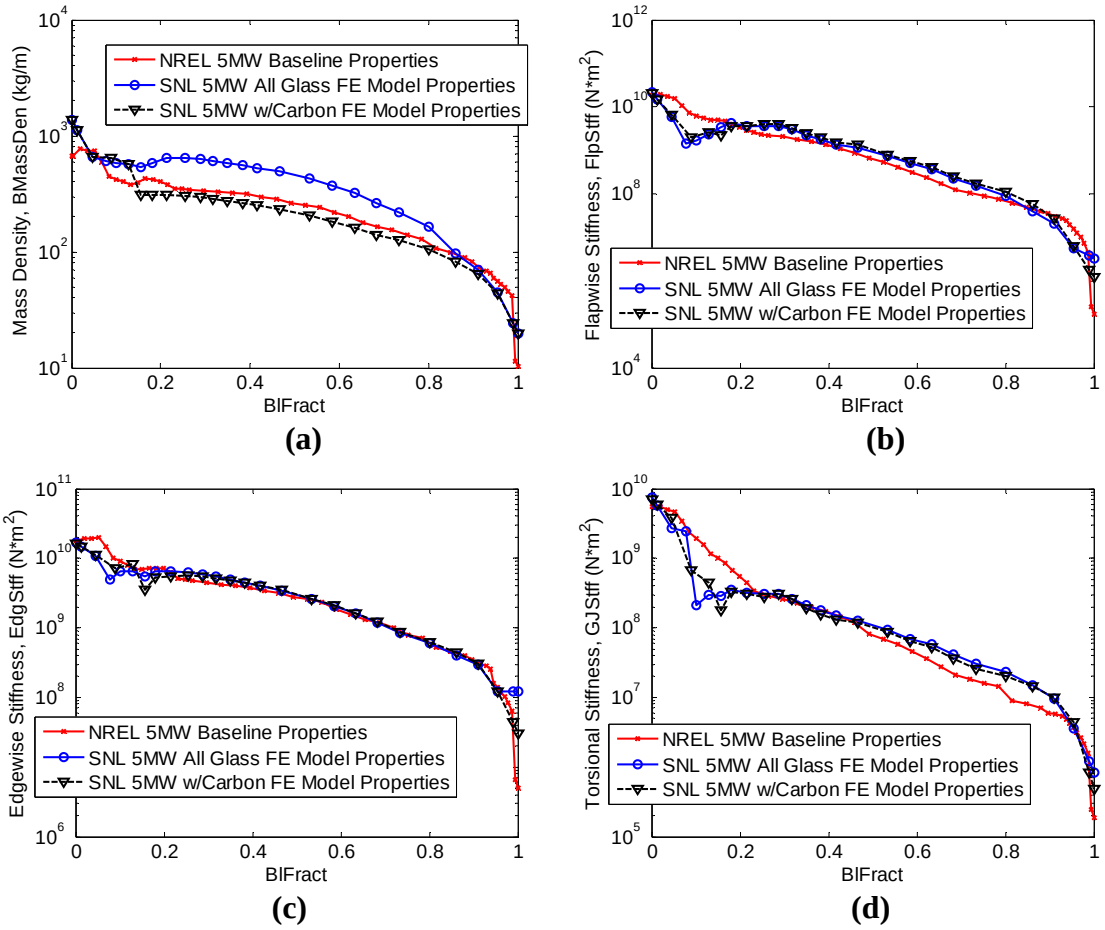


**Figure 9. Blade properties as calculated by BPE including the (a) mass density, (b) flap-wise stiffness, (c) edge-wise stiffness, and (d) torsional stiffness along the span of the blade.**

**Table 2. Summary of estimated mass for each version of the model.**

| | |
|---|---|
| Specified weight of NREL 5-MW Blade | 17,740 kg |
| Fiberglass Blade Model Weight | 25,630 kg |
| Weight of Blade Model With Carbon Spar Caps | 16,381 kg |

## 3.3. Equivalent Beam Property Extraction (BPE)

Blades are complex structural items with span-wise varying shapes, many layers of fiber and resin composite material, sandwich structures and, typically, one or more shear webs (Figure 10). The current approach for wind turbine aeroelastic simulation requires the simplification of this complex wind turbine blade structure into a beam model. Equivalent beam properties of the blade are determined at a discrete number of locations along the span of the blade in order to create a model consisting of several beam elements.

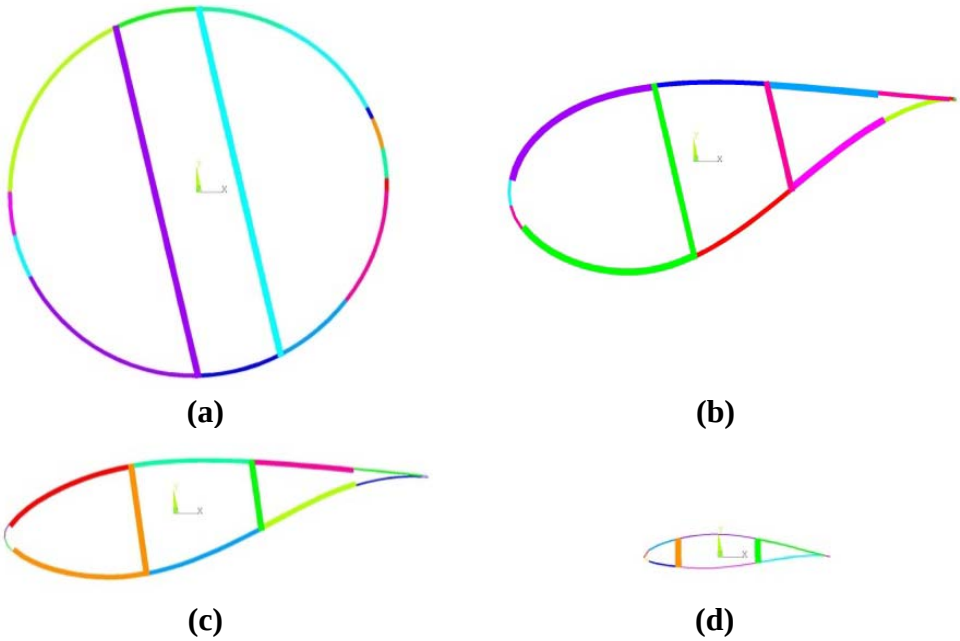

**(a)** **(b)**

**(c)** **(d)**

**Figure 10. Blade cross section shapes for the SNL 5-MW blade model. Colors correspond to different composite layup regions: (a) root, (b) max chord, (c) mid-span and (d) tip.**

Currently there are multiple tools and approaches available to the wind industry that will aid the designer in converting complex blade laminate and structural geometry information into equivalent beam properties for aeroelastic simulations. A common approach is to calculate properties for the Euler-Bernoulli beam based on material properties and skin geometry of each two-dimensional section. The properties at each two-dimensional section are independent of adjacent sections. Simple examples include the following. In addition, warping functions for torsion must be calculated.

$$EI\_flap = \iint E(x,y)x^2 dxdy\,, \tag{1}$$

$$EI\_edge = \iint E(x,y)y^2 dxdy\,, \tag{2}$$

$$GJ = \iint G(x,y)(x^2+y^2)dxdy \quad \text{and} \tag{3}$$

$$EA = \iint E(x,y)dxdy \tag{4}$$

A more involved approach uses a three-dimensional finite element model of the blade and analyzes the deflection of selected nodes in response to applied loads, as seen in Figure 11. Effective properties for Timoshenko beam elements are then determined by analyzing the relative displacements for each pair of adjacent sections. This approach can include effects that are difficult to include in a two-dimensional approach, such as axial warping in torsion and cross-sectional deformation in bending.

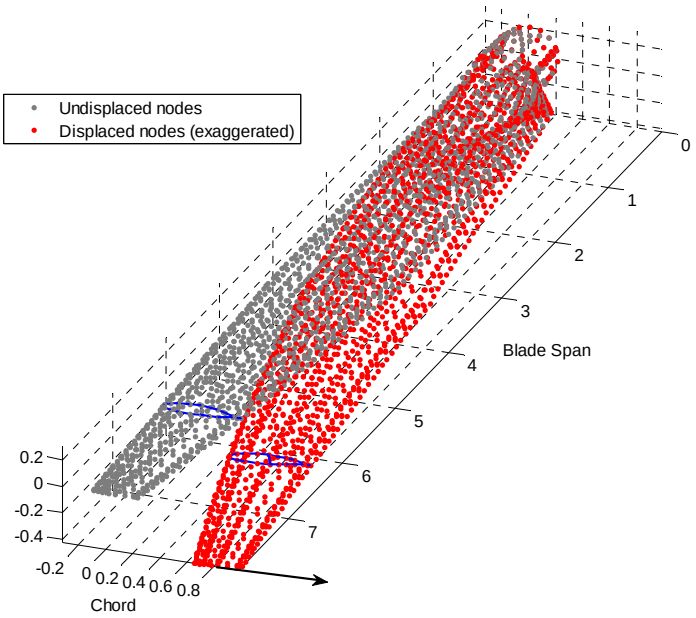


**Figure 11. Finite element nodes: single point edgewise load at the blade tip. A set of finite element nodes representing a blade section is highlighted in blue.**

SNL BPE is a code and a technique to extract equivalent beam properties from a wind turbine blade finite element model [17]. The method is based on applying loads in each of the six degrees of freedom at the tip of the three-dimensional blade model then processing the resulting nodal displacements to generate the 6×6 Timoshenko stiffness matrices for the specified beam discretization. The method; therefore, includes three-dimensional effects such as shear and warping. It also captures effects arising from nearby boundary conditions and non-uniform blade geometry. Calculation of the section properties are demonstrated in a series of validation examples in Malcolm and Laird [17-20]. BPE accommodates blades with curvature in one or both directions and has the ability to identify the center of mass, elastic center, principal directions, shear center and off-axis coupling terms. More discussion of BPE theory and application can be found in references by Laird et.al. [21] and Resor [22, 23].

To improve the overall performance of BPE several small changes were made to the BPE process for its application in this work. The first change was the application of more than six load cases to the ANSYS model. By applying more than six linearly independent sets of loads, the inversion process to determine the equivalent stiffness matrices was overdetermined and the numerical conditioning of the inverse problem was improved. The second change was the incorporation of the beam elements' physical properties directly into the inversion process used to calculate the resulting stiffness matrices. Based on the physical characteristics of the beam elements, each section should have a symmetric positive-definite stiffness matrix. However,

neither the symmetry nor the positive definitiveness of the estimated stiffness matrix is guaranteed through the use of the previously utilized linear least squares inversion. To address this problem, a method that had been developed specifically to determine symmetric positive-definite matrices [24] was used to calculate the resulting 6x6 beam element stiffness matrices for the applied forces and resulting displacements.

The detailed blade model (SNL 5MW) developed for this study is a useful tool for evaluation of local changes in blade structural response for various applied loads. The current work has focused on developing a model that could be used for these initial SHPM scoping studies to direct future work. While the current model is fairly mature, it will also benefit from additional refinements in the future. First, the outboard upper surface (low pressure, LP, surface) spar cap is rather thin and buckles under applied load. This can be dealt with by 1) tapering the width of the spar cap so that it's narrower outboard, 2) adding a foam layer in the LP spar cap to increase thickness and buckling resistance, or 3) adding more layers of UD carbon outboard in the spar cap. This blade design should be evaluated in detail with respect to all certification design load cases. As is, there are certain localized strains that exceed allowed levels under applied load as well as buckling load factors that are low. Both of these issues can be solved with a deeper assessment and redesign of material placement and transition of cross section shapes. Even with the future work desired on this blade model, it is adequate for the SHPM investigation described in the remainder of the report.

## 3.4. Damage Modeling Methodology

To model the presence of a TE (trailing edge) disbond on a wind turbine blade, the NuMAD software was modified so that nodes on the blade TE were split into two different nodes (i.e. TE nodes were unequivalenced). This effectively split the blade model at the TE in a similar way to how the blade is physically constructed by bonding two separate clam shells together. To simulate a healthy TE bond, the top and bottom TE nodes were connected using constraint equations in all six degrees of freedom. In the area of the blade in which the TE disbond existed the constraints were removed so that there was no connection between the top and bottom of the blade. Figure 12 shows an example of the influence of this disbond on the blade's dynamics where the separation of the 1.25 meter long disbond extending from max chord outboard is readily apparent in the first torsional mode shape of the cantilevered blade. While the separation of the TE is clearly visible in the mode shape, it resulted in a decrease in natural frequency of less than 0.01 Hz.

While this modeling methodology effectively models a disbond in which the two sides do not come into contact, it fails to take into account the possible interaction of the top and bottom surfaces of the disbond. For large disbonds in which interaction between the top and bottom of the blade may have a significant influence, the relative decrease in stiffness due to the disbond is likely over-estimated because the added stiffness due to the interaction of the two sides of the disbond is not taken into account. Modeling the interaction between the two surfaces could be achieved using nonlinear surface contact constraints on both sides of the blade but this was not accomplished during this initial investigation and remains as future work.

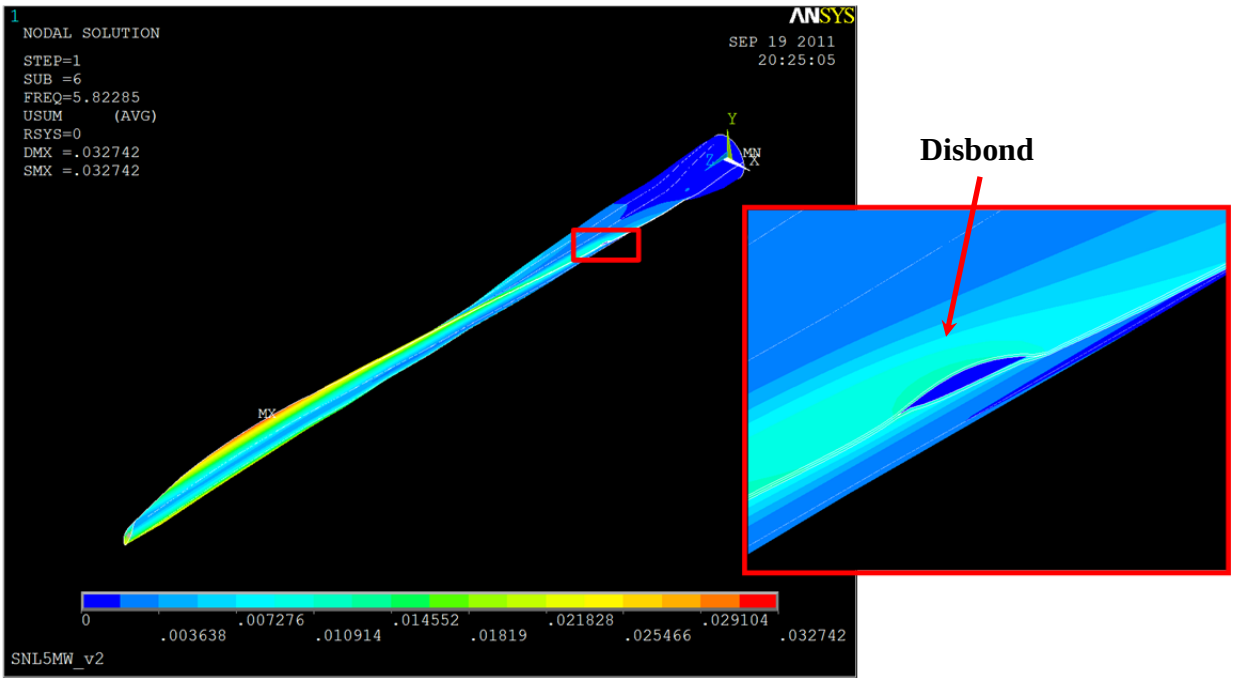


**Figure 12. An image of the first torsional mode shape of a cantilevered blade with a disbond extending 1.25 m from max chord toward the tip of the blade.**

# 4. DAMAGE SENSITIVITY STUDY

In this chapter the developed multiscale modeling methodology is demonstrated through an investigation into the sensitivity of a wide range of potential operational measurements to the presence of a TE disbond. This damage feature was chosen because it is commonly seen in the field [25]. For this initial investigation, all of the disbonds were assumed to have initiated at max chord of the blade (14.35 meters along the span from the root) and propagated outboard toward the tip of the blade.

This chapter begins with an explanation of the results obtained from the reduced order equivalent blade models of the damaged blades that were produced using SNL's BPE technique (Section 3.3) and the physical insight that these results give on the physical effects of the TE disbond. Next a brief example of a local sensitivity analysis that uses the loads from the full turbine simulations is presented that demonstrates the localized nature of the changes in the blade's strain field due to damage. The chapter then concludes with an in depth review of the global sensitivity analysis. The data features that were used to quantify the sensitivity of the operational measurements are presented first and then the results from full turbine aeroelastic simulations in FAST [13] and ADAMS [14] are presented. While, the results from the FAST simulations showed only very slight changes in the operational response of the turbine the ADAMS simulations resulted in far more significant changes. This difference is believed to be due to the fact that ADAMS takes into account the torsional flexibility of the blades while FAST does not.

## 4.1. BPE Five Megawatt Sensitivity Analysis

The creation of a reduced order model for use in full turbine simulations offered the ability to investigate the physical manifestation of the TE disbond on the blade stiffness parameters. To determine which of the span-wise stiffness values calculated using BPE were the most sensitive to the presence of the TE disbond, a series of 37 different blade models were created with disbonds that extended up to 6 meters outboard from max chord. For each of these blade models the equivalent beam stiffness values were extracted using BPE at 23 locations along the span of the blade.

### 4.1.1. *BPE Convergence Analysis*

The first step in the extraction of equivalent beam parameters was to perform a convergence analysis to determine an appropriate mesh seed size in ANSYS to ensure that the parameters extracted using BPE were from a sufficiently converged model. This analysis was performed by calculating the average absolute percent difference in the extracted BPE stiffness values between each candidate seed size and the reference results that were obtained from a mesh seed size that was 1.8% of maximum chord (0.08 m). By calculating the average absolute percent difference of the changes in the estimated EI, EA, and GJ values, changes in all of the estimated stiffness values could be combined into a single convergence metric. The resulting mean absolute percent difference as a function of mesh seed size can be seen in Figure 13 where the mesh seed size is plotted on a log scale. Based on this analysis a mesh seed size of 0.125 m was chosen for future analyses and is highlighted in Figure 13.

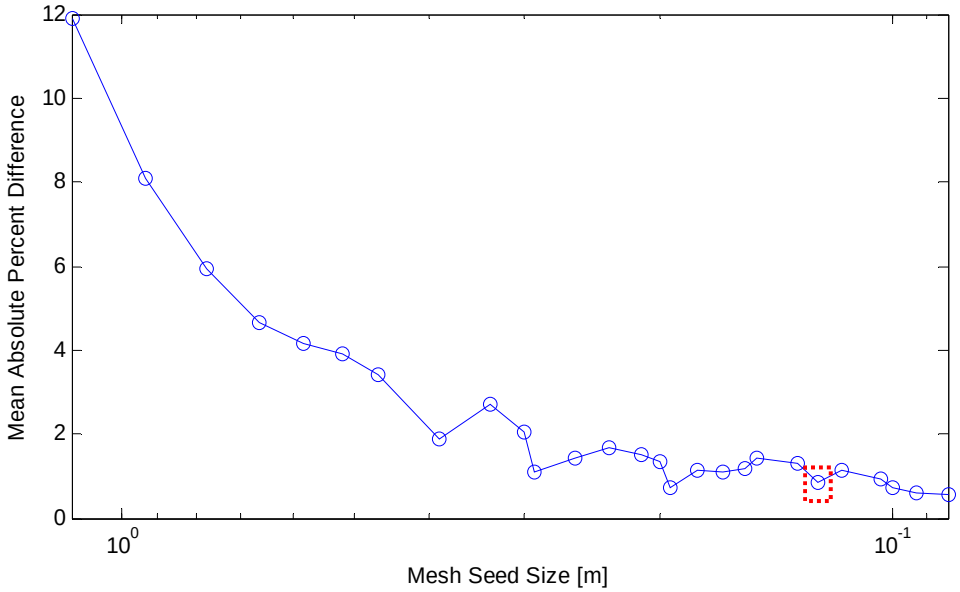


**Figure 13. The mean absolute percent difference in the extracted BPE stiffness values as a function of ANSYS mesh seed size.**

### 4.1.2. *BPE Trailing Edge Disbond Sensitivity*

The sensitivity of the estimated reduced order stiffness values to the TE disbond was quantified by calculating the percent decrease in each of the stiffness values for all of the sections in the reduced order model. The flap-wise and edge-wise bending stiffness values were almost completely unaffected by the presence of the disbond as can be seen from Figure 14. In these plots the percentage decrease in the stiffness of each element is represented by the height and color of the vertical bar where the location of the element and the length of the disbond corresponding to the change are shown on the x-axis and y-axis respectively.

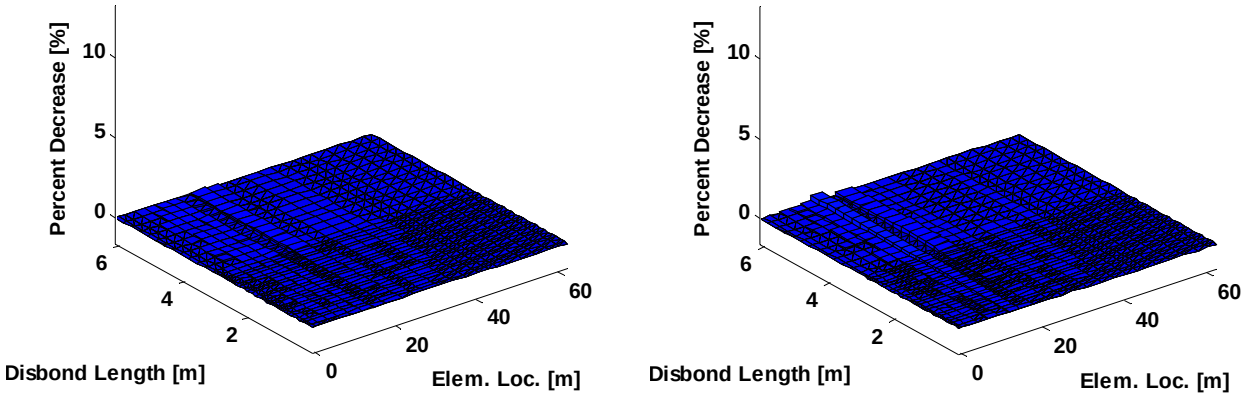


**Figure 14. The percent decreases in the flap-wise (left) and edge-wise (right) stiffness values for segments spaced along the length of the blade and varying length disbonds.**

The axial stiffness values extracted by BPE decrease slightly with the presence of fairly large TE disbonds as shown in Figure 15. For the 6 meter disbond a percentage decrease of 1.8% was seen in the blade section that was just at the outboard end of the disbond. This decrease may

have been due to changes in the three-dimensional warping and shear deformations of the blade that were caused by the presence of the disbond.

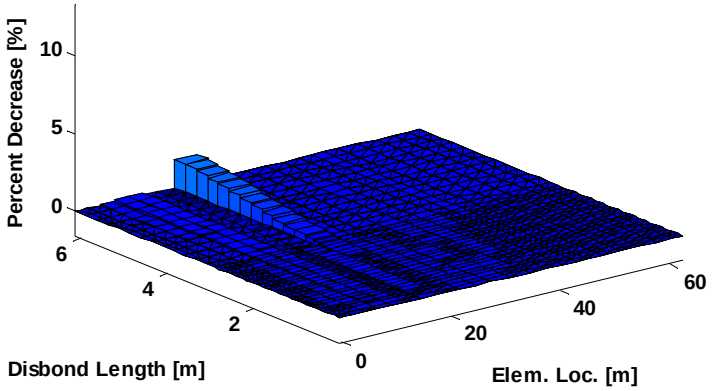


**Figure 15. The percent decrease in the equivalent axial stiffness calculated by BPE due to a TE disbond.**

The disbond had by far the largest effect; however, on the torsional stiffness of the blade sections near the damage as can be seen in Figure 16. In this plot percent decreases of over 13% were seen in the blade sections due to the 6 meter disbond while a 0.625 meter long disbond caused decreases of up to 0.9%. Another pertinent feature of the changes due to damage was that the decreases in the stiffness values were highly localized to the regions in which the disbond was present. The reduction of the reduced order model's torsional stiffness due to the disbond gives physical insight into the problem and suggests that the blade's torsional properties are heavily influenced by the TE disbond.

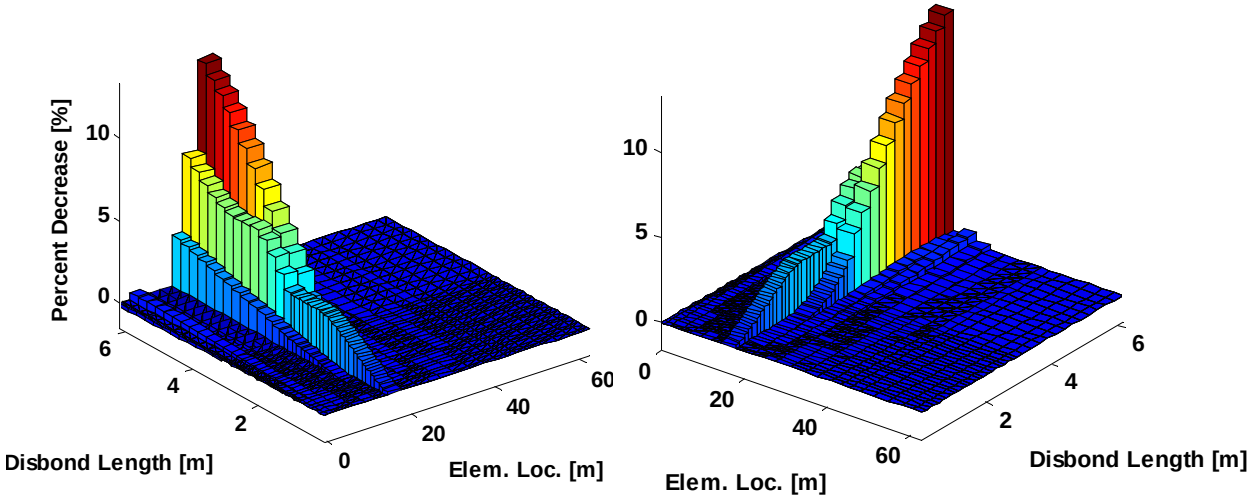


**Figure 16. The percent decrease in the equivalent torsional stiffness of each section due to a TE disbond. Two different views of the same plot are shown to demonstrate the localization of the stiffness changes in the damaged sections of the blade.**

## 4.2. **ANSYS Strain Field Results (Local Sensitivity)**

Aerodynamic loads from the full system aeroelastic simulation can be translated to a set of equivalent forces for application to finite element nodes as a distributed load in the detailed blade model. Figure 17 shows the 5-MW blade model with force vectors representing the steady aerodynamic load for normal operation at 11 m/s, near rated wind speed.

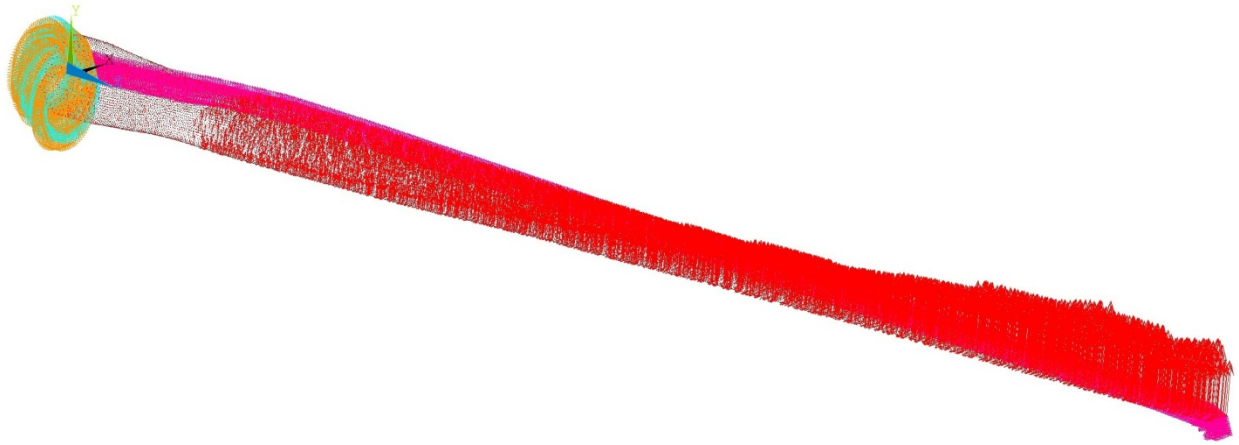

**Figure 17. Force vectors representing aerodynamic load applied to the 5-MW blade finite element model.**

A 0.625 meter long TE disbond, representing just over 1% of blade span, has been modeled in the detailed blade model. The response of the blade structure to the applied aerodynamic forces was computed for both the healthy and damaged blades and localized strains were determined in each element for both scenarios. The difference in strains for each element can be computed in order to see the effects of the damage on the overall blade strain distribution. The difference in blade longitudinal strain (along the span of the blade) between the healthy and unhealthy conditions is shown in Figure 18. The vast majority of the blade does not experience a change in strain due to this magnitude of damage, seen as the color green. Near the disbond at the TE there is evidence of a redistribution of strains, on the order of 50-150 microstrain. While a change in strain of this magnitude could be detected by a strain based health monitoring system, the sensors would clearly have to be located close the location of damage. Furthermore, data normalization procedures would be needed in order to account for variations in the operating temperature, turbine speed, and variations in the aerodynamic forces that naturally occur during turbine operation.

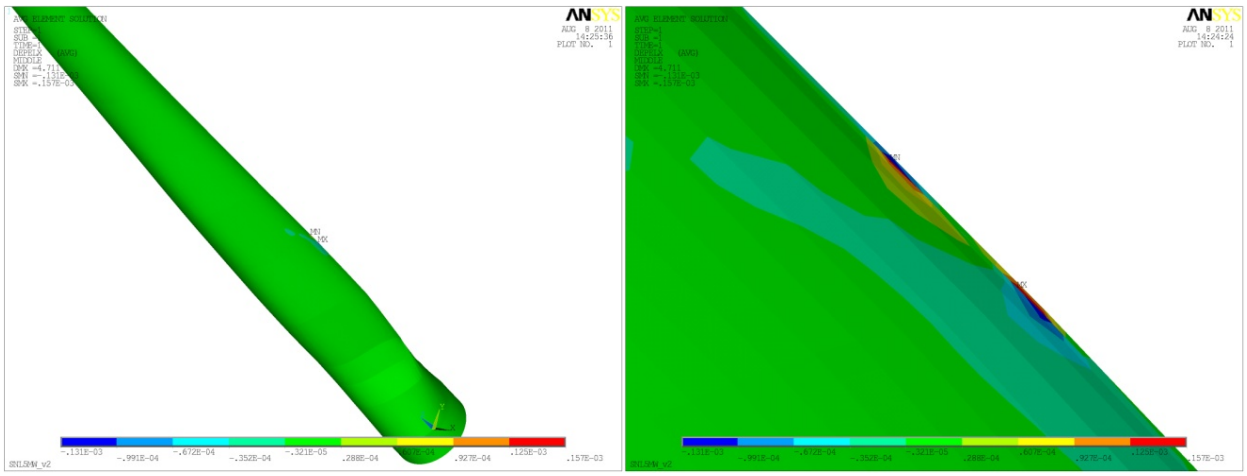

**Figure 18. Graphical depiction of the magnitude of change in longitudinal strain resulting from the presence of a 0.625m long TE disbond located slightly outboard of maximum chord.**

This example has briefly shown the potential for the use of aeroelastic models in computing blade loads, application of loads to the detailed blade model, and analysis of the blade structural response for effects of one type of blade damage. Additional types of damage can be represented in the blade finite element model and evaluated using this process.

## 4.3. Operational Response Results (Global Sensitivity)

Due to the large potential benefits of SHPM a large amount of research in the damage detection and structural health monitoring for wind turbines has been performed in recent years [10, 26-28]. To a large extent the prior work has focused on the application of specific methods or methodologies to a series of different potential problems. Rather than taking this approach to the problem of monitoring the health of offshore wind turbines using operational response measurements, this work approached the problem more generally by using full turbine simulations and simple time domain methods to identify which responses are the most sensitive to the presence of damage. This approach was selected because if the response measurement that is used by SHPM system is unaffected by the presence of damage, damage will not be able to be detected regardless of the sophistication of the damage detection methodology that is used.

To identify the effects of a TE disbond on the operational response characteristics of an offshore wind turbine, both FAST and ADAMS models of the turbine described in Section 3.1 were used in conjunction with seven different blade models. These blade models were developed using the NuMAD and BPE process that was described in Section 3.3. The seven different blade models used in these simulations included one healthy blade model as well as models that included disbonds with length 0.625, 1.25, 1.875, 2.5, 4 and 6 meters. These lengths corresponded to disbonds ranging from approximately 1-10% of the total length of the blade and were a subset of the blade models used in the BPE sensitivity study described in Section 4.1. In the full turbine simulations only a single blade (blade 1) was damaged by changing the reduced order blade model while the two other blades were modeled using the healthy blade model in all of the simulations.

Because the goal of this investigation was not the development of damage detection algorithms but rather the determination of the sensitivity of different measurements to damage; all of the input parameters to the model were kept consistent between the data sets other than the model for the damaged blade. By keeping all of the simulation parameters other than a single blade file constant the sensitivity analysis could be simplified considerably because the changes in the model's output should only be due to the TE disbond. Consequently, the same input wind data file with a mean wind speed of 11.4 m/s and IEC turbulence characteristic A (generated using TurbSim [29]) and selected for all of the simulations.

This section proceeds with an explanation of the data features that were used to quantify the sensitivity of the operational responses. The section then continues with the application of those measures to results from simulations performed in either FAST or ADAMS. Both simulation platforms were investigated because while FAST is able to perform full turbine aeroelastic simulations very efficiently it does not model either the longitudinal or torsional degrees of freedom of the blades. ADAMS simulations, on the other hand, require far more computational time than FAST, but are generally more refined and model both the longitudinal and torsional mass and stiffness characteristics of the blade. Therefore, the ADAMS simulations may be able to more accurately simulate the relatively small and localized changes in the torsional stiffness of the blades due to a TE disbond.

### 4.3.1. *Rotational Resampling and Synchronous Averaging*

In addition to analyzing the output responses of the simulations directly, data normalization through rotational resampling and synchronous averaging was also investigated. This process was performed in order to focus the sensitivity analysis on differences in the turbine's response due to the damaged blade rather than slight differences in the start-up of the turbine. Rotationally resampling is the process of interpolating data so that rather than having data points that are spaced equally in time, the acquired data points are spaced equally with respect to the rotor position (or azimuth angle) and occur at the same rotor position during each rotation.

Once the time histories were resampled, the average responses over an integer number of rotations of the turbine were calculated using synchronous averaging. In synchronous averaging blocks of data are averaged together in which each data point coincides with the same rotor position. This a common practice in the health monitoring of rotating machinery because responses that are repeated every rotation of the system constructively interfere, while random noise and transient events destructively interfere and their influence is minimized. Another benefit of time synchronous averaging using an integer number of rotations of the turbine is that it results in a signal that is nearly periodic. The periodic nature of the synchronously averaged signal reduces the amount of leakage if the signal is transferred into the frequency domain using the Fourier Transform.

However, once the rotational resampling and synchronous averaging procedures have been performed, the response measurements still must be post-processed to obtain a single data feature so that the sensitivity of each channel to the disbond can be quantified. Some sensitivity measures that were applied to the rotational resampled and synchronously averaged data or the raw time histories will now be discussed.

### 4.3.2. *Sensitivity Measures Investigated*

The sensitivity of a function is generally defined as the partial derivative of that function with respect to the variable of interest. In this case, however, the sensitivity of a response time history with respect to a change in a model must be computed, which is slightly more involved because it requires the condensation of the changes in the time history into a single data feature. Nonetheless several key aspects of how to define the sensitivity of a measurement can be derived from its definition for a function. The first, and most obvious, is that the measured response should change when the variable of interest is changed. For the present simulations this means that the time histories from the damaged model must be different in some way from the time histories generated by the healthy model. Secondly, the change in the time history should be in some way correlated to changes in the length of the disbond. Therefore; in the following analyses, channels will be defined as sensitive to the presence of the TE disbond if they are changed by the presence of the disbond and the change tends to increase as the size of the disbond increases. Furthermore, because the focus of this analysis was on the physics-based determination of the measurements that were the most sensitive to damage, only simple time based damage features have been investigated.

#### 4.3.2.1. Statistical Moments

The first data feature that was used to assess the sensitivity of operational response measurements to the disbond were the statistical moments of the data. This data feature was only extracted from the raw time histories. These parameters were tracked because changes in the moments are correlated to changes in the underlying distribution of the data which may be caused by damage. The investigated moments included the mean, variance, skewness and kurtosis of the data. While the mean and variance of the data are well known measures of the expected value of the data and the spread of the data respectively, the skewness and kurtosis are less well known statistical moments that can be used to help describe the shape of the distribution.

The sample skewness [30] is an estimate of third standardized moment of a distribution and is defined as,

$$\hat{\tau} = \frac{\frac{1}{n}\sum_{i=1}^{n}\left(x[i]-\bar{x}\right)^3}{\left(\frac{1}{n}\sum_{i=1}^{n}\left(x[i]-\bar{x}\right)^2\right)^{3/2}} \tag{5}$$

where $i$ is the index of the time point, $n$ is the total number of data points and $\bar{x}$ is the sample mean of the data. The skewness is a measure of the asymmetry of a distribution where a positive skewness value indicates that there are relatively few values that are larger than the mean but those large values are relatively far away from the mean.

The sample kurtosis [30] is an estimate of the fourth standardized moment of a distribution and is defined as,

$$\hat{\kappa} = \frac{\frac{1}{n}\sum_{i=1}^{n}\left(x[i]-\bar{x}\right)^4}{\left(\frac{1}{n}\sum_{i=1}^{n}\left(x[i]-\bar{x}\right)^2\right)^2} \tag{6}$$

again where $n$ is the number of data points and $\bar{x}$ is the sample mean of the data. Large values of kurtosis indicate that while a significant portion of the data is in a relatively narrow range there are also several large outliers. Therefore, the kurtosis can also be thought of as a representation of the "peakedness" of a distribution. Kurtosis is a widely used damage detection measure in the field of rotating machinery [31].

#### 4.3.2.2. Standardized RMS Difference

Due to the fact that the only variation between the models was the presence of the TE disbond, the sensitivity of the model's responses could theoretically be calculated by directly calculating the differences between the healthy and damaged response time histories. To gauge the difference in the responses the root mean square (RMS) of the difference between the healthy time histories and the damaged time history was computed for each channel. However, if the magnitude of the signal itself is not taken into account in this investigation, the magnitude and the units of the response will influence the results. Therefore to normalize the data and create a unitless measure of sensitivity, the RMS differences were standardized by dividing the difference for each channel by the standard deviation of that data from the healthy blade. This sensitivity metric can be written for the $j^{th}$ test as:

$$\Delta_j^{RMS} = \frac{\sqrt{\frac{1}{n}\sum_{i=1}^{n}\left(x_j[i]-x_0[i]\right)^2}}{\sqrt{\frac{1}{n}\sum_{i=1}^{n}\left(x_0[i]-\bar{x}_0\right)^2}} \tag{7}$$

where $i$ is the index of the time point, the subscript represents the test the data is from with 0 indicating the healthy data, $n$ is the total number of time points and $\bar{x}_0$ is the mean of the healthy data. While this process would not work for data that was a constant throughout the healthy simulation, all of the data of interest in this investigation was dynamic data.

Despite the straightforward nature of applying this approach to the raw time histories, a small difference early in the simulation can lead to a phasing differences between simulations that propagate throughout the entire duration and leads to anomalous indications of damage sensitivity. Because of these phasing issues, this data feature may be more useful when applied to the rotationally resampled and synchronously averaged data where any phasing differences were compensated for using the resampling procedure.

#### 4.3.2.3. Maximum Standardized Mean Difference

In addition to facilitating synchronous averaging, rotationally resampling the data allows the changes in the response data at a given rotor position to be investigated. Therefore, to create this damage sensitivity metric rather than synchronously averaging the rotationally resampled data to obtain the average waveforms (as was the case when the standardized RMS analysis described above was applied to the synchronously averaged data) the distribution of the resampled data at a given rotation angle was analyzed. The damage sensitivity metric that was used in this work was the difference between the synchronously averaged waveforms divided by the standard deviation of the healthy data at each rotor position. This measure of sensitivity will be referred to as the maximum standardized mean difference and can be expressed for the $j^{th}$ test as:

$$\Delta_j^{MAX} = \max_\theta \left( \frac{\bar{r}_j[\theta] - \bar{r}_0[\theta]}{\sqrt{\frac{1}{n_r}\sum_{i=1}^{n_r}\left(r_{0,i}[\theta] - \bar{r}_0[\theta]\right)^2}} \right) \tag{8}$$

where $\bar{r}_j[\theta]$ is the synchronously averaged data for the $j^{th}$ test at the rotation angle (azimuth position) $\theta$, $r_{0,i}[\theta]$ indicates the data from the healthy turbine during the $i^{th}$ rotation, $n_r$ is the total number of rotations in the healthy data set, and $\max_\theta$ indicates that the maximum is taken across all rotation angles. This sensitivity measure was chosen because it emphasizes differences in responses that are relatively consistent for a healthy turbine but changes due to the presence of damage.

### 4.3.3. *FAST Simulations*

Due to the desire to investigate the sensitivity of a wide range of different measurements to the TE disbond, 199 different response outputs were obtained from FAST. More outputs would have been investigated but at the time the study was performed FAST had a limit of 200 output parameters for a single test. A variety of different measurements were obtained on the turbine's rotor including the local accelerations and moments in three directions on blades 1 and 2 at the nine locations spaced along the span of which are shown in Figure 19. The same measurements from blade 3 were not acquired because they were assumed to be similar to those from blade 2 (also simulated as an undamaged blade) and were therefore not included in the analysis so that alternative measurements could be investigated. A variety of measurements that were not on the rotor were also acquired including the local tower accelerations and loads at 4 different locations on the tower. A variety of measurements from the turbine's drive train were also measured including the nacelle IMU translations and rotations, the generator speed, power and torque, as well as a variety of forces and moments from the low speed shaft.

The first response sensitivity metric that was applied to the FAST data were changes in the statistical moments of the response data. The mean, standard deviation, skewness and kurtosis for each of the 199 channels were calculated. Because the magnitude of the statistical moments can vary depending on the units of the underlying data, in order to compare the sensitivity of

multiple channels of data which may have different units, the percent change in each of the moments was also calculated.

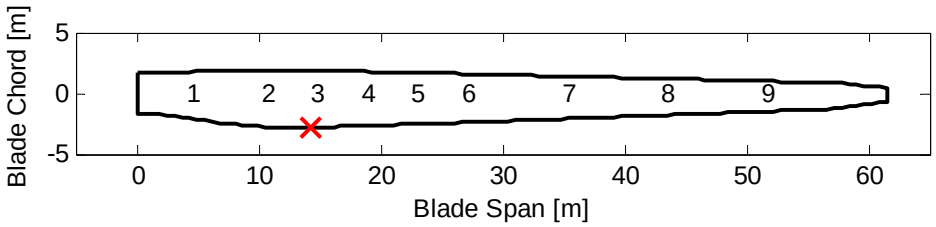


**Figure 19. The locations of the local acceleration and moment measurements along the length of the blade. All of the investigated disbonds extend outboard from max chord which is indicated with a red "X".**

Despite the fact that the mean of the responses were relatively unaffected by the presence of damage, several channels did show some slight changes in their mean values due to the damage. Some of the measurements that had small (<1%) changes in the mean of the data were the pitching moments on the damaged blade which progressively decreased with an increase in the length of the disbond. However, the mean of the low speed rotating shaft shear force that was directed perpendicularly to the length of the shaft changed the most in a relative sense and was correlated with the damage state. A bar chart showing the mean of this measurement channel for the healthy blade (damage state 0) all of the investigated disbond lengths (damage states 1-6) is shown in Figure 20 and the slight increase in the mean with the increasing length of the disbond is evident.

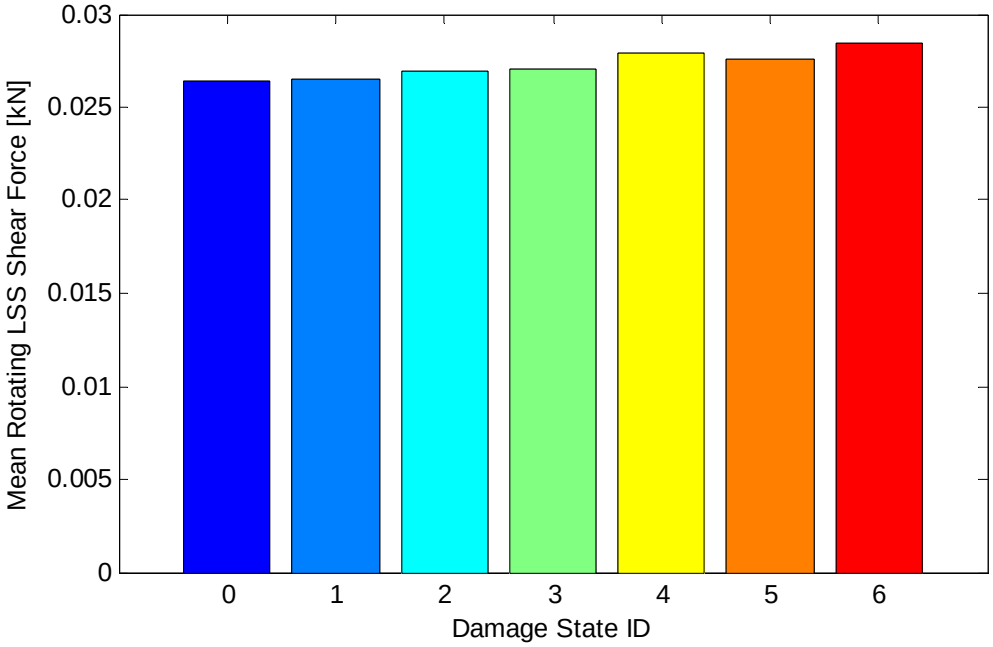


**Figure 20. The mean rotating shear force in the low speed shaft for 7 turbine models. The damage states from 0 to 6 are the healthy blade and the blades with a 0.625, 1.25, 1.875, 2.5, 4, and 6 meter long disbond respectively.**

While the largest percentage change in the mean of the data was not on the rotor, changes in the higher moments of the data that were correlated with the size of the disbond largely occurred in the measurements on the blade. The data that registered the largest and most consistent percent changes were the local pitching moments on the damaged blade near the damage location. The absolute percentage changes for the skewness of the pitching moments along the blade are shown in Figure 21 while the absolute percentage changes in the kurtosis of the data are shown in Figure 22. The z-axis on these plots indicates the absolute percentage change in the data while the x-axis indicates the measurement location ID (see Figure 19 for the locations) and the y-axis is the damage state. The large erratic absolute percent differences in the skewness for measurement location 1 are believed to be due to that fact that the skewness of the response near the blade root was almost zero and therefore the relatively small changes were magnified disproportionately. Note that the scale on the vertical axis of these two plots are different and that the most significant change on the statistical moments on the blade that was correlated with the damage state of the structure was the change in the skewness of the pitching moments near the location of the disbond.

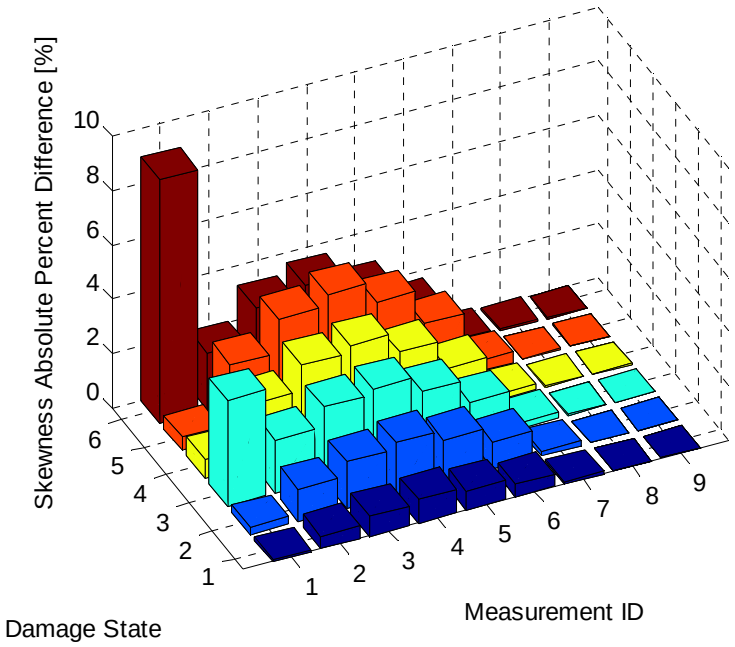


**Figure 21. The absolute percent change in the skewness of the pitching moments along the length of the blade for the 6 different damage states. The damage states 1 through 6 correspond to disbonds of length 0.625, 1.25, 1.875, 2.5, 4, and 6 meters respectively.**

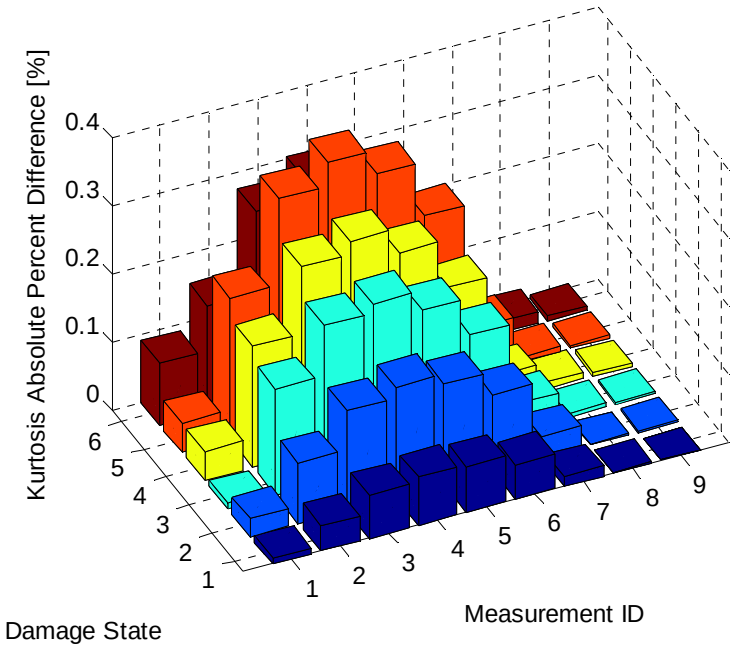


**Figure 22. The absolute percent change in the kurtosis of the pitching moments along the length of the blade for the 6 different damage states. The damage states 1 through 6 correspond to disbonds of length 0.625, 1.25, 1.875, 2.5, 4, and 6 meters respectively.**

When the standardized RMS difference methodology was applied directly to the FAST output data the data channel with the largest difference was found to be the azimuth, or rotor position. While this may be due to a change in the blade model, the second largest standardized difference was due to smallest (0.625 meter) disbond. Therefore, it is believed that this difference is due to slight changes in the response of the turbine during start-up which resulted in a slight shift in the position of the turbine.

When the standardized RMS difference (Section 4.3.2.2) was performed after the data had been rotationally resampled and synchronously averaged (Section 4.3.1) using a single rotation of the turbine, the data channels with the largest standardized sensitivity to the damage are the accelerations along the damaged blade in the edge-wise direction. A contour plot showing the magnitude of the standardized RMS difference for all nine of the edge-wise accelerations and each of the damage conditions is shown in Figure 23. Note that the largest absolute RMS differences do not occur for the most severe damage level but rather come about due to the 4 meter long disbond, which was also the case for skewness and kurtosis. For the majority of the locations and disbond lengths investigated, however, the differences in the time history increase as the length of the disbond increases and the most sensitive accelerometers are those near the location of the disbond. However, these differences are a product of very small differences in the response time histories as can be seen by a plot of the time history corresponding to the edge-wise accelerations measurements at 36.35 meters (Figure 24). This relatively small changes in the accelerations suggests that while some differences are observable in the overall average accelerations these changes would most likely be exceedingly difficult to detect in a real-world situation assuming that the FAST simulations accurately model the effects of the TE disbond on the turbine's responses.

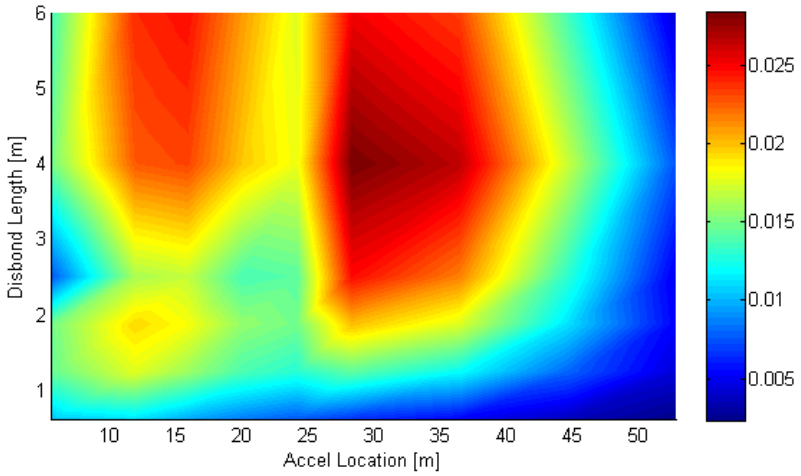


**Figure 23. The standardized RMS difference in the edge-wise accelerations of the damage blade. The x-axis shows how the difference changes along the length of the blade while the y-axis shows how the difference is influenced by the length of the disbond.**

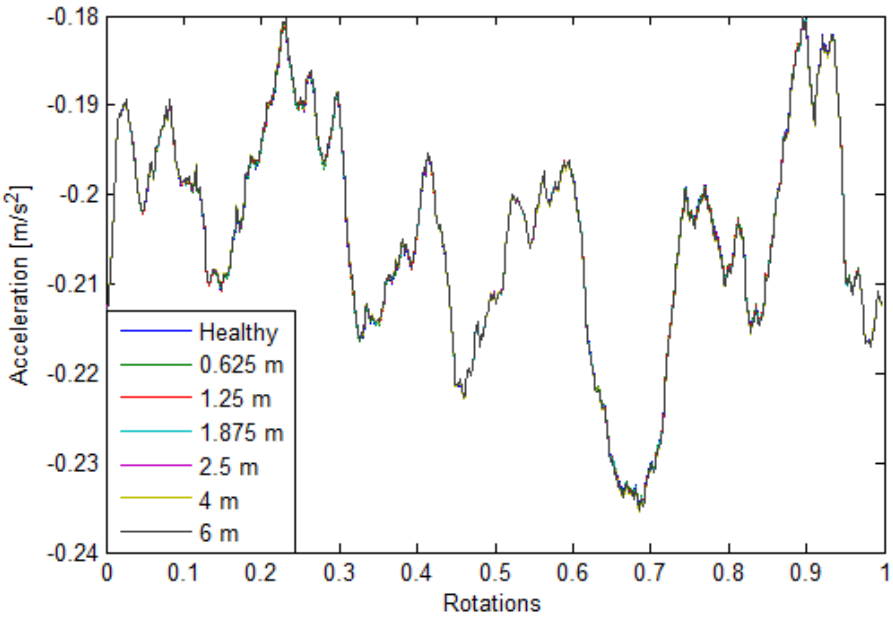


**Figure 24. The average edge-wise accelerations at 36.35 meters for all 7 of the FAST models. Only very small differences between the responses are evident.**

Using the maximum standardized mean difference the response channel with the largest sensitivity to damage was the local pitching moment on the damaged blade. A surface plot of the magnitude of the maximum standardized mean difference for all nine of the measurement locations where the local pitch moment of the blade was measured for each of the 6 different damage conditions is shown in Figure 25. Note that once again the largest differences do not occur for the most severe damage level but rather are seen for the 4 meter long disbond. Figure 26, however, shows that while the localized differences may increase with damage only very small differences are actually present in the time histories which once again suggests that

detecting these changes in the presence of variable loading or environmental factors would be very difficult.

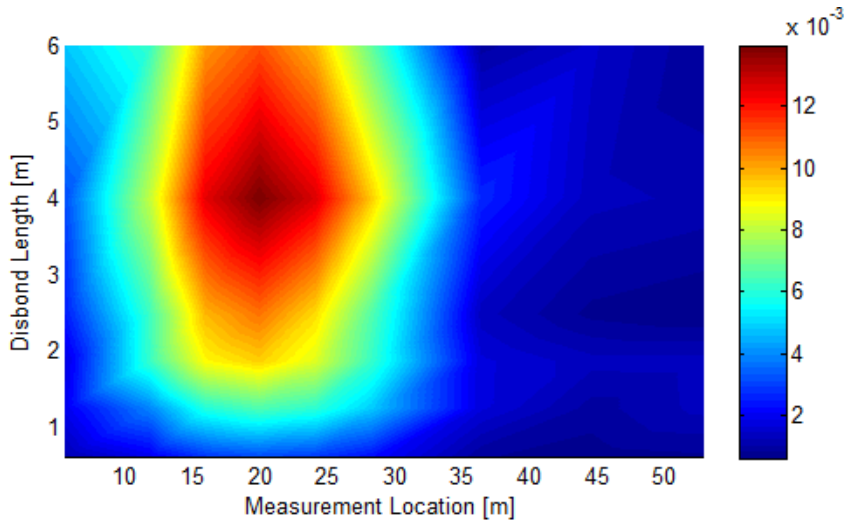


**Figure 25. The maximum standardized mean difference in the damage blade's pitching moments. The x-axis shows how the difference changes along the length of the blade while the y-axis shows how the difference is influenced by the length of the disbond.**

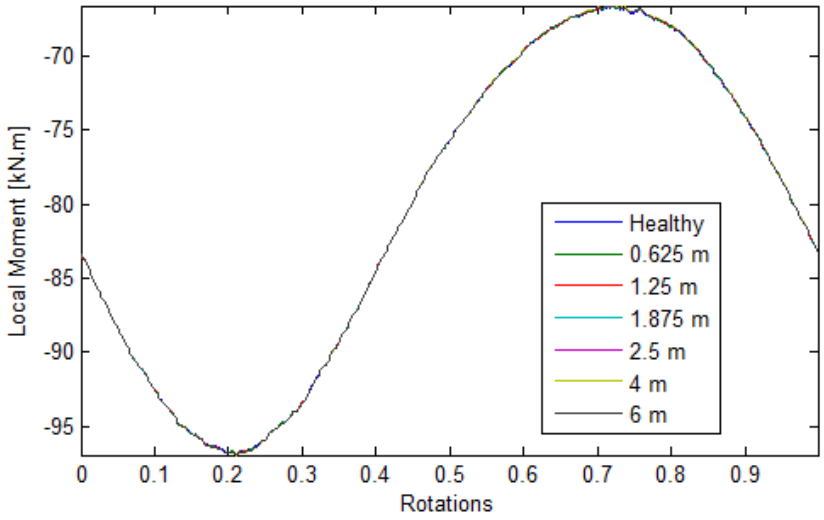


**Figure 26. The average pitching moment at 20 meters for all 7 of the offshore FAST models. Only very small differences between the responses are evident.**

While several different methods have been applied to the results of FAST simulation to determine operational responses that are sensitive to the presence of a TE disbond no significant changes in the turbine's response due to the disbond were found. However, the FAST simulations may not be appropriate for an investigation of the effects of a TE disbond because the blade's torsional degrees of freedom are not modeled in FAST. This is especially significant because the BPE sensitivity analysis found that the torsional stiffness of the blade was significantly affected by the presence of the TE disbond while the edge-wise and flap-wise degrees of freedom were relatively unaffected. Therefore, the operational sensitivity analysis was also conducted using an ADAMS model as detailed in the next section.

### 4.3.4. *ADAMS Simulation Results*

Because the blade's torsional degrees of freedom could not be modeled in the FAST simulations, the FAST preprocessor was used to create an ADAMS model of the offshore 5-MW turbine which allows both the pitching and span-wise flexibility of the blade to be included in the model. As with the FAST simulations, 30 seconds of start-up data at the beginning of each simulation was discarded and the remaining hour of response data was acquired and analyzed. Furthermore, because ADAMS has no limit on the number of requested outputs a much larger candidate set of output responses could be investigated. A total of 1,007 different responses were recorded using a 100 Hz sampling rate for each of the simulations and all of the responses were analyzed to determine their sensitivity. These included the translational and rotational accelerations of all 17 lumped masses for each blade as well as the local forces and moments in each direction. Because of the limitations of the FAST post processing scripts, a new set of requests were added to the generated ADAMS models in order to obtain the equivalent responses directly from ADAMS. The locations of the response measurements along the span of the blade are shown in Figure 27. The translational and rotational forces and accelerations were also recorded at 21 evenly spaced locations along the height of the tower. A variety of other generator, nacelle, and other measurements were recorded and the most sensitive measurements will be described. Each of the simulations took over 8 hours to run on a Dell laptop with two Intel Core2 Duo x64 2.6 GHz processors, 8 GB of RAM, and a 7200 RPM 500 GB hard drive.

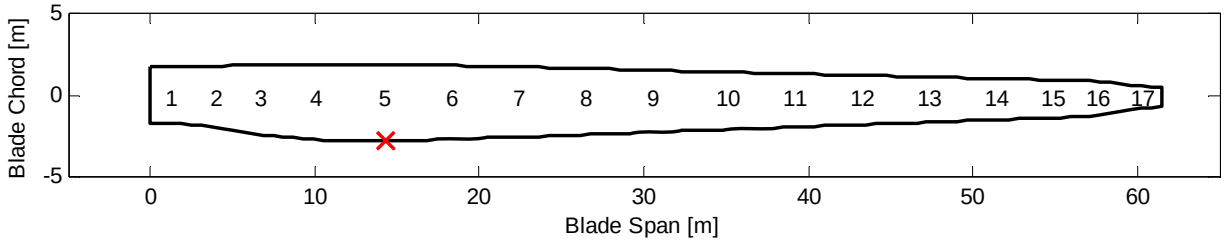


**Figure 27. The 17 measurement locations on each of the blades used for the ADAMS models. All of the investigated disbonds extend outboard from max chord which is indicated with a red "X".**

The preliminary step in this analysis was to determine an appropriate step size for the simulation methodology investigated. Based on work by White [32] the integrator selected for this analysis was the SI2 GSTIFF integration method. While this integrator was found to reduce the number of spurious peaks in the acquired acceleration signals, in this work it was not able to eliminate them using the integrator time step that was used in the FAST simulations. Therefore a convergence analysis was performed based on the maximum integrator step size used for the SI2 integration method. To create a dimensionless convergence metric the RMS difference between the time histories from the smallest step size (1E-4 seconds) and each candidate step size was calculated. However, in order to ensure that the responses with different units were accounted for equally, the difference of each response was normalized by the reference responses' standard deviations and the mean of these values across all of the channels was used as the convergence criteria and is shown in Figure 28. Based on this analysis, a step size of 1E-3 seconds was chosen because it appeared to reduce discontinuities in the time acceleration time histories and was a good compromise between accuracy and computation time.

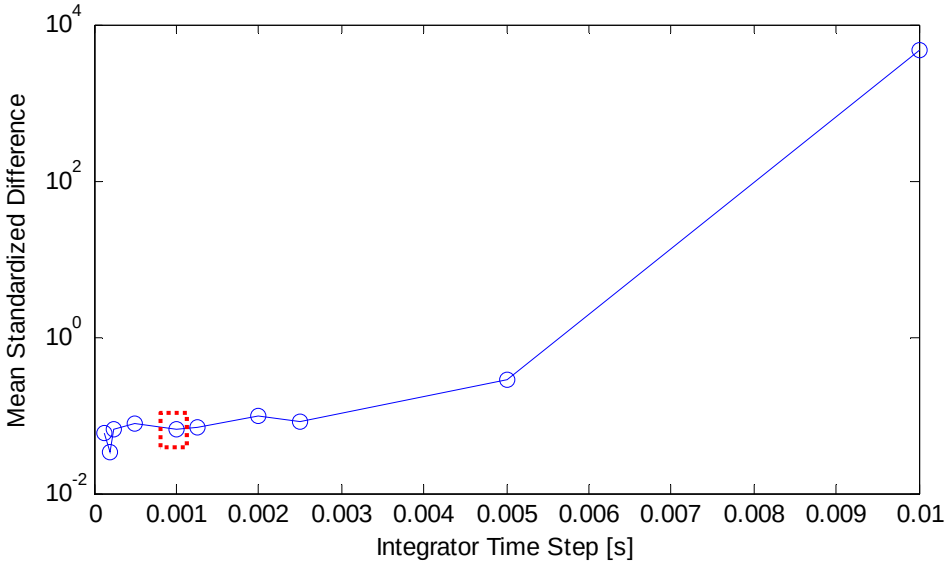


**Figure 28. The convergence metric used to evaluate the integrator step size used in the ADAMS simulations.**

The statistical moments of the responses from the ADAMS simulations of the offshore turbine showed significant percent changes but the majority of them did not exhibit consistent trends with respect to the length of the disbond. The cause of these inconsistent trends is currently unknown and due to the issues previously encountered with discontinuous accelerations, displacement and velocity measurements will be investigated in future simulations. The standardized RMS differences of the time histories were also investigated but as with the moments, the majority of the differences did not appear to correlate well with the extent of the damage.

However, the statistical moments of the pitching moments on the damage blade were well correlated with the presence and extent of the TE disbond and displayed significant percent changes in some cases. Figure 29 contains a three dimensional bar chart of the absolute percent different in the mean of the pitching moments along the span of the damaged blade due to the six different disbond lengths investigated. Note that two views of the plot are shown in the figure in order to demonstrate the span-wise variations in the changes. The mean pitching moments on the element centered at 15.85 meters down the span of the damaged blade changed up to 4% due to the disbond and in general the changes in the mean seem to generally increase with increasing length disbonds. These changes are over four times larger than those seen in the FAST simulations which is believed to be due to the fact that ADAMS takes into account the torsional flexibility of the blades while FAST does not.

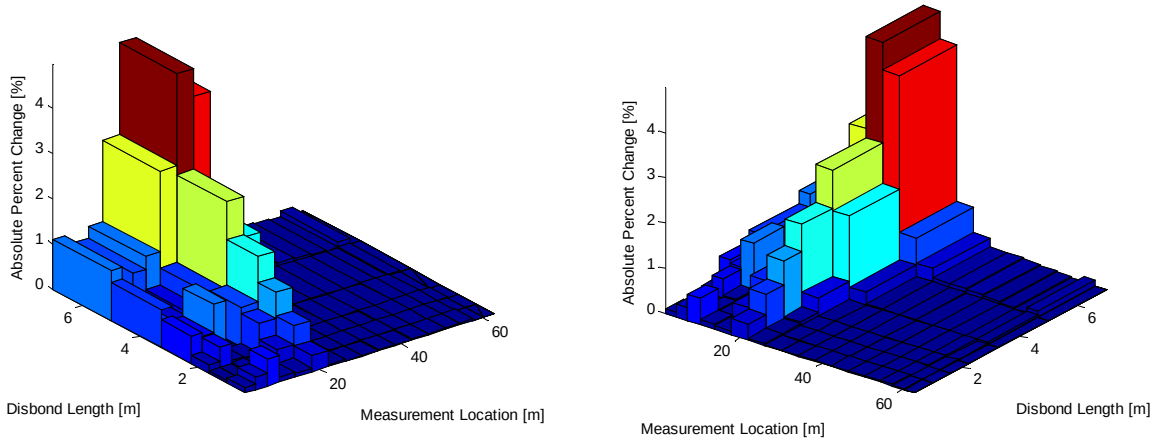


**Figure 29. Two views of the absolute percent change in the mean of the pitching moments along the span of the damaged blade due to TE disbonds between 0.625 and 6 meters.**

In addition to changes in the mean, the changes in the standard deviation, skewness, and kurtosis of the damaged blade's pitching moments were also well correlated with the size of the disbond. The changes in the standard deviation of the pitching moments are shown in Figure 30 and show even larger percent changes due to the disbond than did the mean of the data with changes of up to 20% for the 6 meter disbond. While the changes in the mean of the data also occurred near the root of the blade the differences in the standard deviation of the pitching moment were highly localized around the damage location.

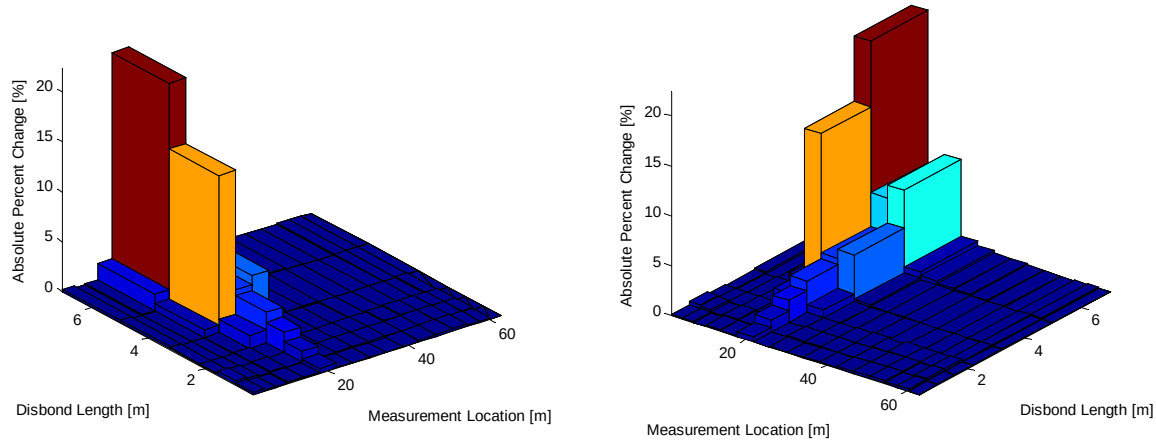


**Figure 30. Two views of the absolute percent change in the standard deviation of the pitching moments along the span of the damaged blade due to TE disbonds between 0.625 and 6 meters.**

The percent changes in the skewness of the data (Figure 31) were over 300% and were even more localized than the changes in the standard deviation. However, it should be noted that the healthy skewness values were fairly small which resulted in exaggerated percent differences. Changes in the kurtosis of the data were also localized around the damage location but only exhibited percent differences that were slightly larger than 10% as can be seen in Figure 32. *The consistent changes in all four of the statistical moments investigated shows that the pitching*

*moments around the damage location are highly influenced by the TE disbond and should be included in an SHPM system designed to detect this form of damage.*

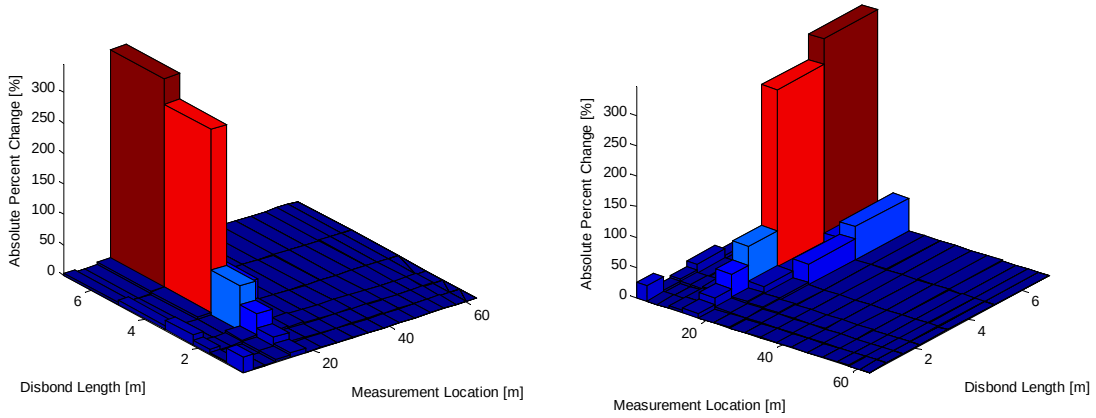


**Figure 31. Two views of the absolute percent change in the skewness of the pitching moments along the span of the damaged blade due to TE disbonds between 0.625 and 6 meters.**

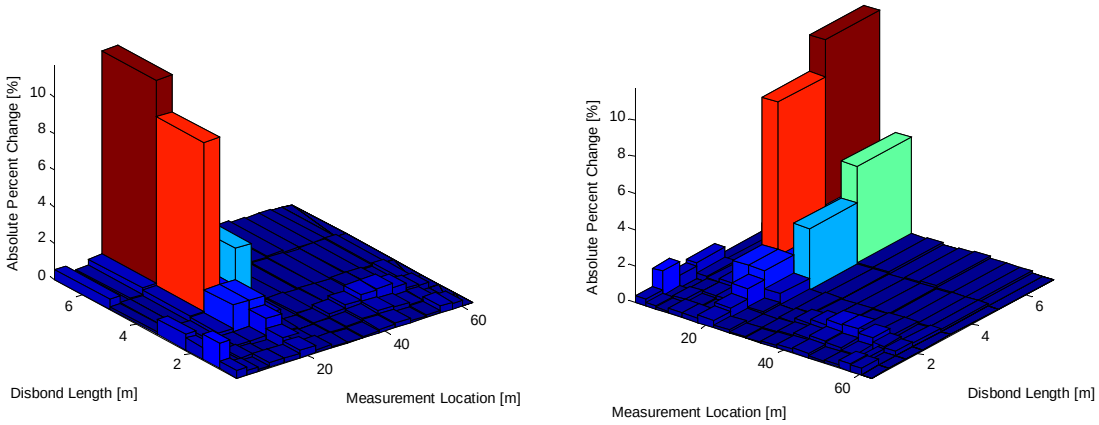


**Figure 32. Two views of the absolute percent change in the kurtosis of the pitching moments along the span of the damaged blade due to TE disbonds between 0.625 and 6 meters.**

To focus the sensitivity analysis on the operational response of the turbine, the rotational resampling and synchronous averaging technique described in Section 4.3.1 was performed on the ADAMS response measurements. When the standardized RMS difference (Section 4.3.2.2) of the average waveforms was utilized to determine the influence of the disbond on the models' responses, the responses with the largest changes between simulations were not correlated with the size of the disbond in the model. However, out of the channels of data whose standardized RMS difference was correlated with the disbond size, the pitching moments in the damage blade demonstrated by far the most significant differences. The RMS difference in the average waveforms generated from the pitching moments on the damaged blade are shown in Figure 33. RMS differences of over 9 kN•m were seen due to the 6 meter disbond, consistently increased with the length of the disbond, and were once again well localized around the location of the damage.

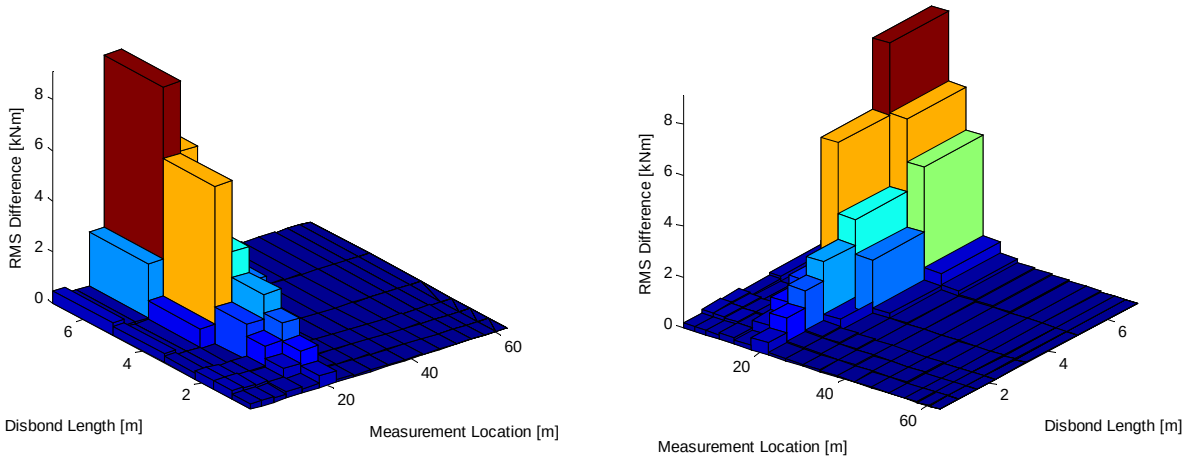


**Figure 33. Two views of the RMS differences in the average pitching moments along the span of the damaged blade due to TE disbonds between 0.625 and 6 meters.**

When the sensitivity of the rotationally resampled time histories was quantified using the standardized mean difference at different rotation angles (Section 4.3.2.3), the most sensitive measurements were once again found to be the pitching moment near the location of the disbond. A set of three dimensional bar charts (Figure 34) shows that the maximum standardized mean difference shows changes due to damage beginning with the 0.625 m disbond and that these differences increase as the length of the disbond increases. In this case the largest difference between the average waveforms is over 0.6 times the standard deviation of the healthy data. This maximum difference occurs in the blade section centered around 15.85 meters when the turbine is approximately 1/4 of the way through its rotation, as can be seen in Figure 35. Figure 35 also demonstrates, however, that relatively small changes are seen in this time history due to smaller length disbonds. However, the pitching moments in the next outboard section (centered around 19.95 meters) show differences even for the smallest disbond and these differences increase relatively consistently as the length of the disbond grows (Figure 36).

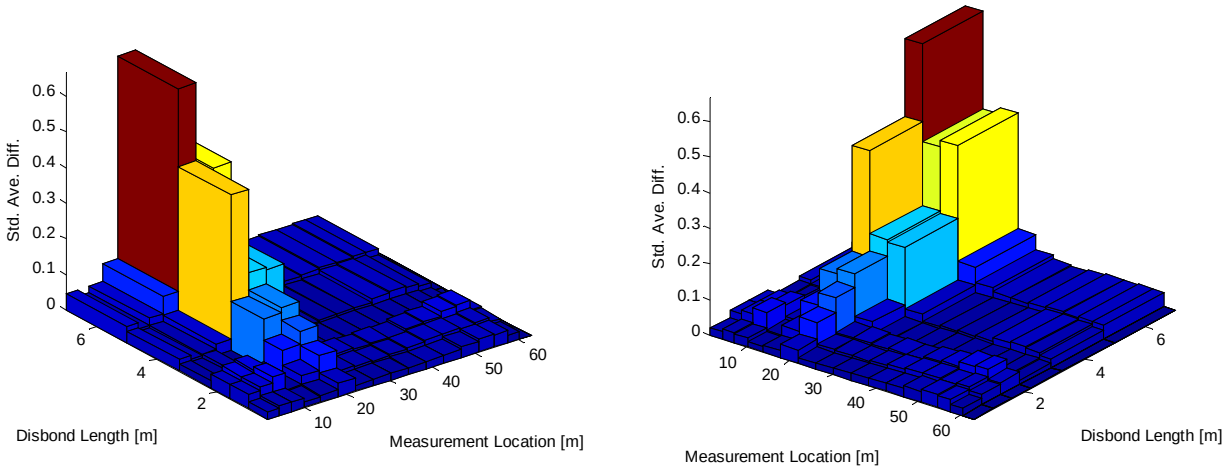


**Figure 34. Two views of the maximum standardized mean difference in the pitching moments along the span of the damaged blade due to TE disbonds.**

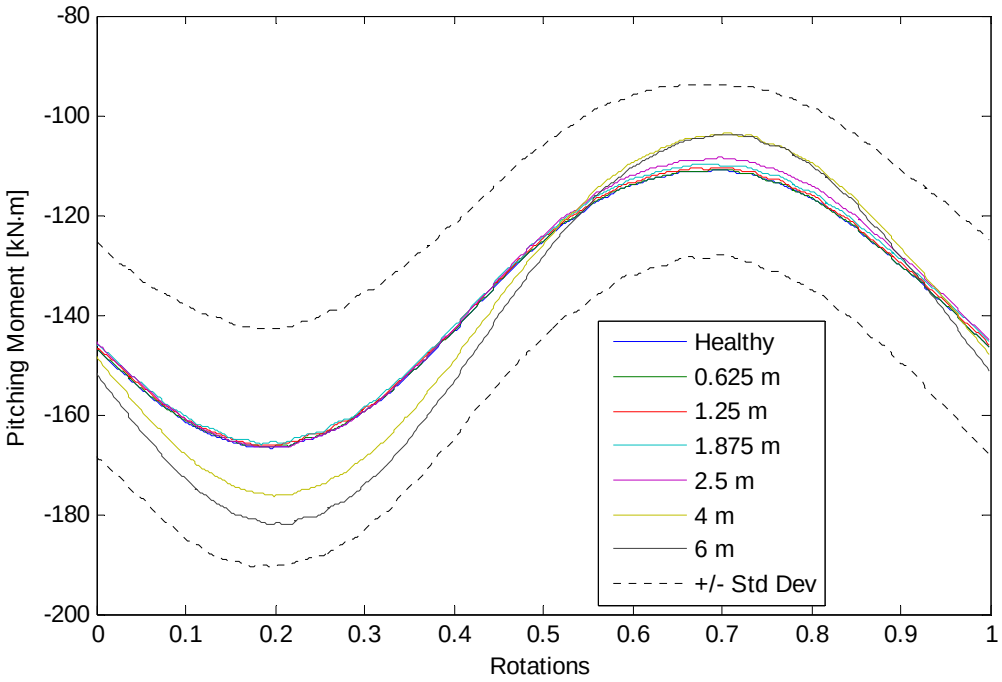


**Figure 35. The average net pitching moment during one rotation of the turbine for a section centered around 15.85 m down the span of the damaged blade for all disbond lengths. The dotted lines are the healthy average pitching moment plus and minus one standard deviation.**

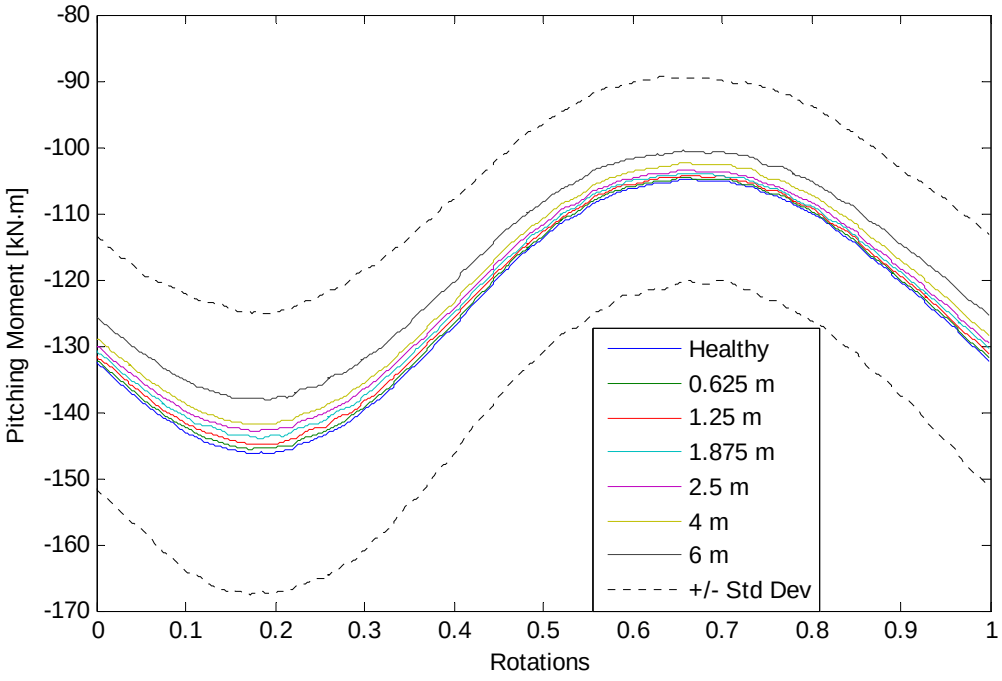


**Figure 36. The average net pitching moment during one rotation of the turbine for a section centered around 19.95 m down the span of the damaged blade for all disbond lengths. The dotted lines are the healthy average pitching moment plus and minus one standard deviation.**

Rather than simply taking the maximum standardized mean difference of the data, an alternative way to investigate the differences in the averaged data is to estimate the distribution of the data at a given rotation angle and quantify differences between the two distributions. In order to estimate the probability density function of the data, a Gaussian kernel density estimator [33] was used. An example of the changes in the estimated distributions due to damage is shown in Figure 37 which contains the probability density estimators of local pitching moment at 15.85 meters when the turbine is a quarter of the way through its rotation. The estimated distribution clearly changes for the larger damage levels as both the center and the spread of the distribution is significantly altered when the disbond is 4 or 6 meters in length.

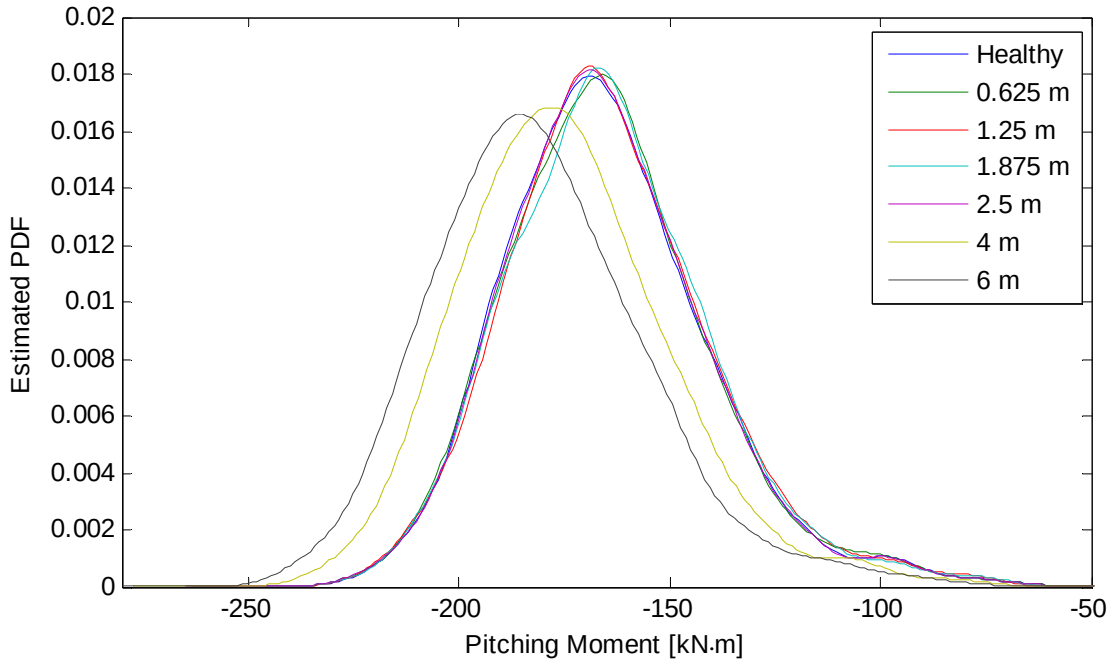


**Figure 37. The probability density estimates generated using the local pitching moment one quarter of the way through a turbine rotation in the section of the damaged blade centered at 15.85 meters and all disbond lengths.**

One way in which the significance of the differences between the distributions can be investigated quantitatively is using a two-sample t-test which tests the null hypothesis that two sets of independent random samples from normal distributions have equal means but unknown and possibly unequal variances. The tests were performed using the Matlab® Statistics Toolbox and the results generated from the pitching moments at 0.25 rotations from the blade section centered at 15.85 m are shown in Table 3. These data shows that the only disbond lengths for which the probability of the two distributions having the same mean was less than 5% were the 4 and 6 meter long disbonds. However, based on the data from the hour of averages the probability of either of these damage cases being from the healthy distribution is less than 4E-12%. Lastly, the 95% confidence interval on the difference between the healthy data and the data from the blade with the 4 meter disbond was between 7.34 and 12.4 kN•m while for the 6 meter long disbond that difference increased to between 13.3 and 18.5 kN•m. While the underlying data used for these tests is non-normal (as is clear through the extended right tail of the distribution) these very low probabilities and large differences in the mean indicate the significance of this change.

**Table 3. The results of the two-sample t-tests using the pitching moment at 15.85 down the span of the damaged blade comparing the data from the healthy blade to the data from each of the disbond lengths.**

| Disbond Size | Reject Hypothesis | P-Value of Test | 95% Difference Confidence Interval |
|---|---|---|---|
| 0.625 | No | 0.88 | -2.70 to 2.31 |
| 1.25 | No | 0.58 | -3.22 to 1.79 |
| 1.875 | No | 0.52 | -3.32 to 1.69 |
| 2.5 | No | 0.99 | -2.51 to 2.47 |
| 4 | Yes | 4E-14 | 7.34 to 12.4 |
| 6 | Yes | 4E-32 | 13.3 to 18.5 |

While the pitching moments from the section centered at 15.85 meters changed significantly for the 4 meter and 6 meter long disbonds, they were unable to statistically differentiate other damage states from the response of the healthy blade. When the probability density estimates were generated from the pitching moments of the blade section centered at 19.95 meters; however, smaller but more consistent changes were evident as shown in Figure 38. To investigate the significance of these changes two-sample t-tests were then performed as described in the previous paragraph. While the hypothesis of significantly different means cannot be rejected with 95% confidence for the 0.625 and 1.25 meter long disbonds the t-test indicates significantly different means for all of the larger disbonds as shown in Table 4.

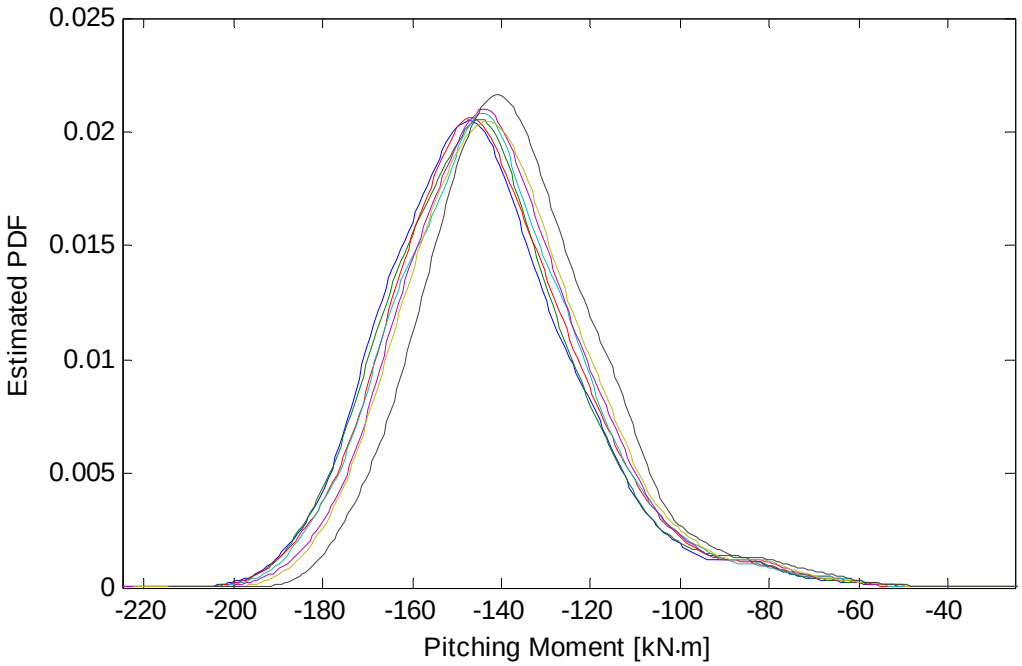


**Figure 38. The probability density estimates generated using the local pitching moment one quarter of the way through a turbine rotation in the section of the damaged blade centered at 19.95 meters and all disbond lengths.**

**Table 4. The results of the two-sample t-tests using the pitching moment at 19.95 down the span of the damaged blade comparing the data from the healthy blade to the data from each of the disbond lengths.**

| Disbond Size | Reject Hypothesis | P-Value of Test | 95% Difference Confidence Interval |
|---|---|---|---|
| 0.625 | No | 0.59 | -2.84 to 1.61 |
| 1.25 | No | 0.18 | -3.74 to 0.69 |
| 1.875 | Yes | 0.046 | -4.48 to -0.0445 |
| 2.5 | Yes | 0.0027 | -5.57 to -1.17 |
| 4 | Yes | 1.19E-4 | -6.52 to -2.12 |
| 6 | Yes | 2.37E-12 | -10.0 to -5.66 |

Using a variety of different methods the sensitivity of the local pitching moments around the damage location to the presence of a TE disbond has been demonstrated and consequently these measurements would be advantageous to have in any SHPM designed to detect the presence of these disbonds. While in this case no off-rotor responses showed significant sensitivity to damage, other types of damage that have a larger effect on the underlying strength of the blades may impact these measurements more significantly and therefore the influence other commonly seen damage mechanisms should be investigated in the future. Furthermore, this example has illustrated the utility of the developed multiscale modeling methodology in the identification of measurements that are sensitive to a particular form of damage and the construction of an SHPM system.

# 5. OPERATIONS AND MAINTENANCE OF A SMART OFFSHORE WIND FARM

## 5.1. Progressive Damage and Cost Function Model

To effectively integrate an SHPM system into the overall O&M strategy for an offshore wind energy plant the repair costs associated with damage should be characterized. While some investigations of CBM implementations [34, 35] use a constant repair cost for each component, a the likely repair cost versus damage size function is expected to be more similar to a piecewise function where different types of repairs have different costs associated with them. Such a curve is shown for blade repairs in Figure 39 and will be employed in future cost-benefit analysis for structural health monitoring. There are four distinct regions of the cost model:

1. Small defects which do not need to be repaired
2. Moderate defects which can be repaired up-tower
3. Large defects which require the blade to be removed
4. Very large defects which require blade removal and replacement

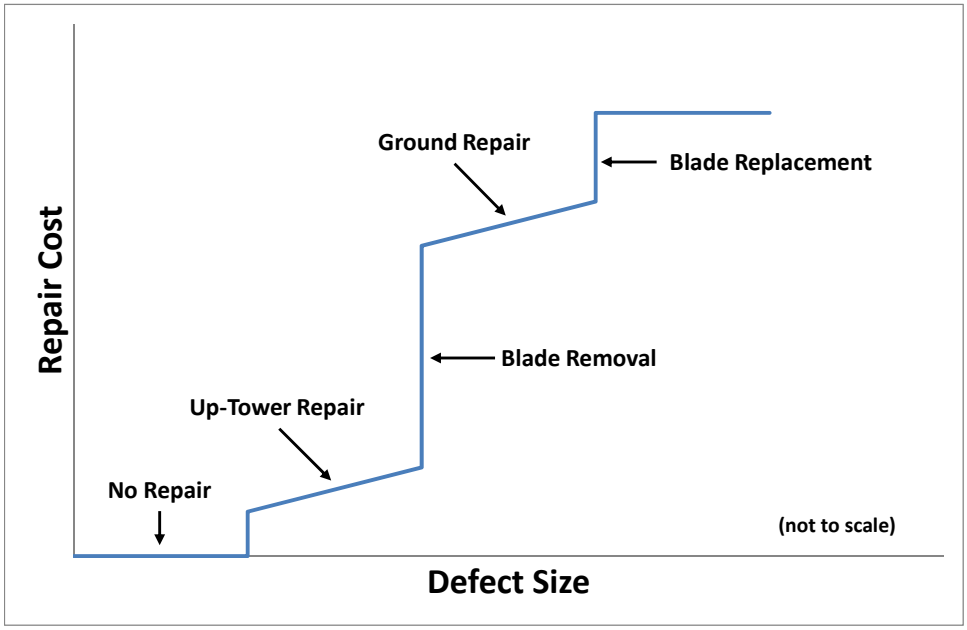


**Figure 39. Example defect-cost model demonstrating the piecewise nature of defect size versus repair cost.**

The exact numbers for this model have not been determined to date, nor has the relationship between repair cost and such factors as defect location, blade size, etc. However, the impact of this cost model in the SHPM cost-benefit analysis would be to show that knowledge of the damage state and the expected future loads would allow an intelligent controller to limit damage growth and keep it within the lower cost regions of the above curve until the repairs can be made. Furthermore, if a damage mitigating control strategy can be developed the turbine could continue to produce revenue even in this degraded state.

## 5.2. **Mitigation of Damage Growth by Turbine Derating**

Next we consider a simple example to evaluate the potential of mitigating wind turbine blade damage by derating the turbine. The presence of a disbond, a crack, or similar damage in the blade can cause a stress concentration which, if high enough, will become the dominant failure point in the blade structure. Due to the cyclic nature of wind blade loads, with time the higher stresses near the crack will exceed allowable levels and will lead to more rapid damage propagation.

### 5.2.1. *Stress Increase Due To Blade Damage*

A very simplified example is shown here in order to demonstrate the concept of stress amplification resulting from the presence of blade damage, in this case a simple crack. If one assumes that a crack is present in the blade such that the crack has an elliptical shape, is oriented perpendicular to applied stress, and is a relatively long crack with small crack tip radius of curvature, then the stress concentration factor associated with the crack is represented by Equation (9)

$$K_t = \frac{\sigma_{\max}}{\sigma} = 2\left(\frac{a}{\rho}\right)^{1/2} \tag{9}$$

where $\rho$ is the crack tip radius of curvature and $a$ is the half length of internal crack.

Making some assumptions about the crack tip radius, one can get a basic sense of the trends and magnitude of stress concentration factors associated with the damage. The stress concentration factor is highly dependent on the crack tip geometry and increases most rapidly for smaller crack lengths as seen in Figure 40. This trend highlights the importance of detecting cracks at early stages.

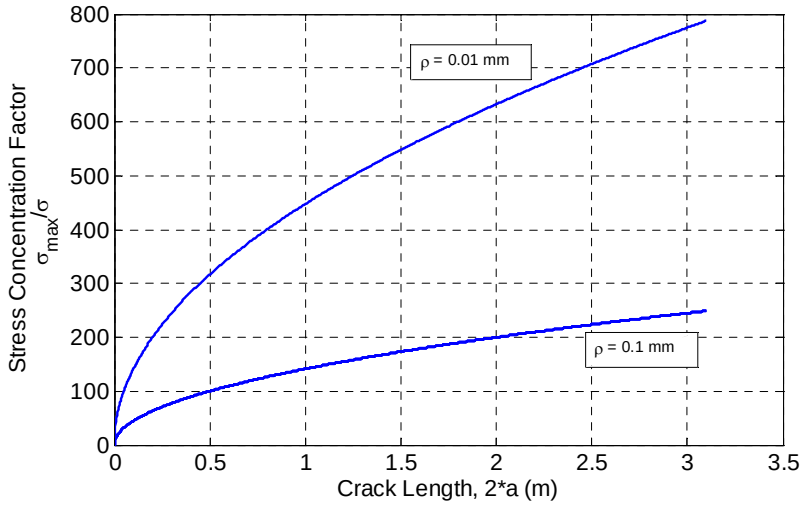


**Figure 40. Stress concentration factors, $K_t$, as a function of crack length; shown for two different crack tip radii, rho.**

### 5.2.2. *Fatigue Life Considerations*

An important blade design driver is fatigue life. The fatigue life of wind blade materials can be estimated using Miner's Rule which has the form:

$$Damage = \sum_i \frac{n_i}{N_F(\gamma_f \gamma_m S_i)} \leq 1.0 \tag{10}$$

where $\gamma_f$ and $\gamma_m$ are partial factors of safety for loads and materials, respectively; specified by design standards, $n_i$ is the number of cycles at cyclic stress level $S_i$, $N_F$ is the number of cycles to failure at the given stress level, and the material is said to have failed when the Damage summation exceeds unity.

The number of cycles to failure, $N_F$, depends on material properties derived from fatigue testing and can be modeled using a wide variety of different methods. One such model is the simple two parameter model for fatigue damage which can be written as:

$$N_F = \left(\frac{1}{C} S\right)^{-b} \tag{11}$$

While more elegant, multi-parameter fatigue life models may be easily inserted for $N_F$ at this point in the analysis process, the simple two parameter model was used in this investigation to gain an initial understanding of the problem.

The damage computed using Miner's Rule can be linearly extrapolated to unity in order to arrive at an estimated fatigue life span of a material. Similarly, the damage for two different stress states can be compared in order to arrive at an estimate of the relative change in fatigue life. Consider the simple example of a 0.5m crack with 0.1mm crack tip radius. Equation (9) and Figure 40 would indicate a stress amplitude increase by a factor of 100 in the material nearest the crack. The ratio of fatigue damage for the blade with the crack and the healthy blade is an indicator of the expected change in fatigue lifetime. The proportional increase in the amount of damage due to the crack can be computed by using equation (11) to determine the number of cycles to failure and simplifying equation (10):

$$\frac{Damage_{cracked}}{Damage_{healthy}} = \frac{\left(\sum_i \frac{C^{-b} n_i}{S_{cracked}^{-b}}\right)}{\left(\sum_i \frac{C^{-b} n_i}{S_{healthy}^{-b}}\right)} = \left(\frac{S_{cracked}}{S_{healthy}}\right)^b = K_t{}^b \approx 100^{12} = 1 \cdot 10^{24} \tag{10}$$

This magnitude of increase in fatigue damage would equate to an enormous decrease in fatigue lifetime for the material near the crack. In reality, this causes failure of the material and thus

growth of the crack. An important question is whether the crack growth accelerates toward complete failure or slows toward a steady state. The hope is that the SHPM system will be able to detect and estimate the size of damage so that the turbine can be controlled to mitigate damage growth and prevent catastrophic failure.

### 5.2.3. *Structural Impacts of Turbine De-Rating*

If the structural loads in the blade can be reduced in the presence of damage, then the propagation of damage can be slowed. One means to reduce loads in the blade is to reduce the energy capture of the turbine, i.e. to derate the turbine. With derating, the turbine experiences lower aerodynamic and structural loads. The result is a decrease in production, but it may be more advantageous to sacrifice some production capacity in the near term in favor of greater benefits in the long term as will be explained in Section 5.3.

Figure 41 shows a simulated distribution of fatigue damage for the 5-MW turbine. Each data point on the curve is computed using Equation (10) above. Stress cycles are found using rainflow counting of time waveform simulation data using Crunch [36] on data generated from aeroelastic simulations that were performed using FAST. The fatigue damage was calculated based on a Rayleigh wind distribution with average wind speed of 10 m/s, representative of an IEC Class I site. The data clearly show that maximum fatigue damage occurs as the turbine is operating in wind speeds that are slightly above 12m/s, the rated wind speed for this machine.

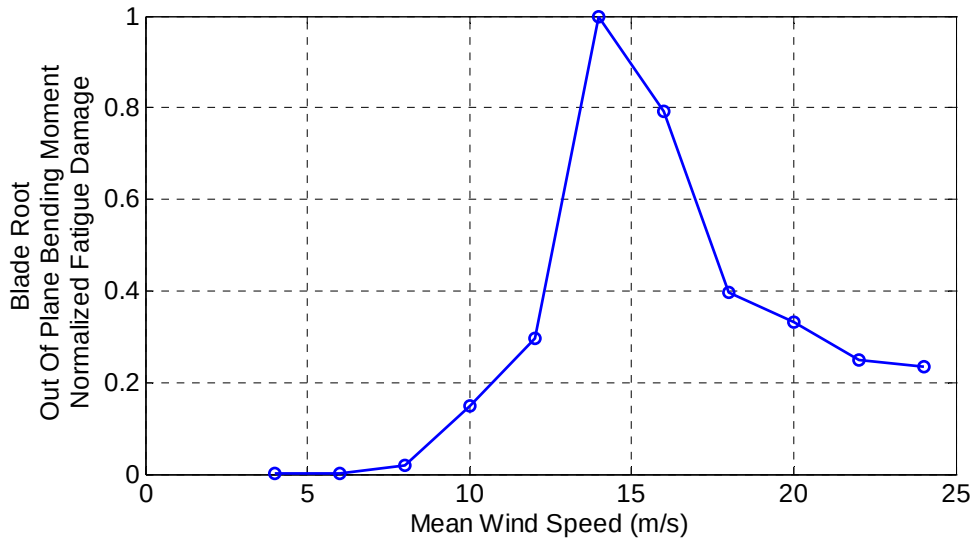


**Figure 41. Fatigue damage distribution at operational wind speeds; blade root bending moment.**

In the presence of damage, it could be beneficial to reduce the turbine loads in the vicinity of the peak in Figure 41 to slow the growth of the damage. This may be done through derating the turbine. Derating the turbine can be achieved through multiple methods, and a small subset of the possible methods is shown in Figure 42 where the control law is varied based on the wind speed region in which the turbine is operating. Mode 1 represents a decrease in the allowable rotor torque in Region 3 and unmodified operation in Region 2. Mode 2 represents a decrease in

allowable rotor torque in Region 3 as well as a decrease in rotor torque in Region 2, which may achieved through feathering the blades in Region 2. Mode 3 represents an entirely new approach where low and high wind speed operation and energy capture remain unaffected. In Mode 3 the turbine is derated only in the vicinity of the Region 2.5 transition, thus affecting only the highest operational fatigue loads. Design and implementation of Mode 2, Mode 3 and other more advanced prognostic control actions is an area for future research.

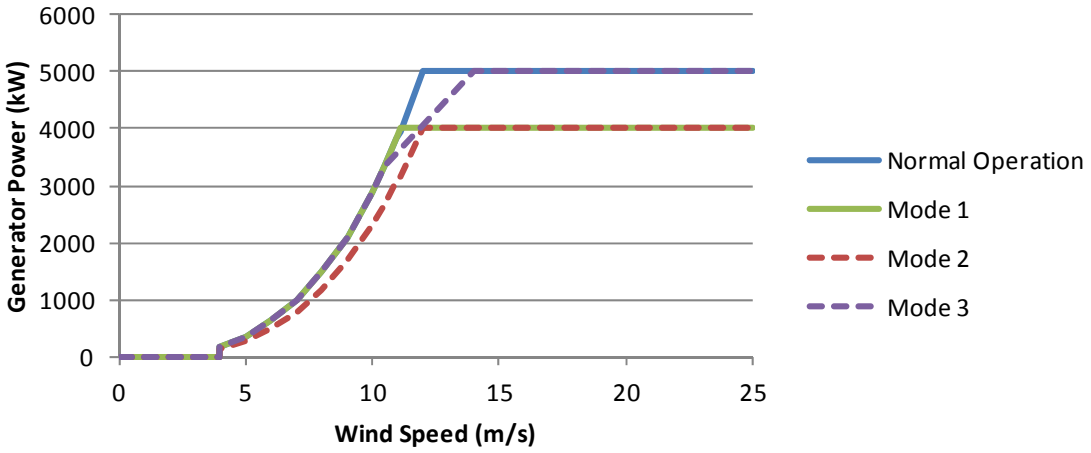


**Figure 42. Illustration of various turbine derating schemes; curves for Modes 1, 2 and 3 illustrate 80% turbine rating.**

It is helpful to analyze the effect of derating a turbine on the cyclic fatigue loads that are encountered on the blade. Figure 43 (a) shows the change in equivalent cyclic load experienced by the blade as a function of turbine rating. Figure 43 (b) shows the change in actual fatigue damage (inversely related to fatigue life) as a function of turbine rating when the Mode 1 derating method was used. Again, the data points in these simulations were generated by FAST and Crunch, using the fatigue analysis process described previously in this report. Derating to 95% leads to a reduction in cyclic loads to levels that are 90% of the rated levels. In addition, it leads to fatigue damage that is 30% of what was incurred at the rated level. Such a decrease in fatigue damage is equivalent to an increase in the fatigue life of the blade by a factor of more than three. The decrease in blade stress resulting from derating will help offset the stress concentrations that arise due to the presence of damage as shown in Figure 40. More significant derating leads to more impressive extension of expected fatigue life. Clearly, an optimization of turbine energy capture versus maintenance costs is required and will provide more understanding regarding an appropriate level of turbine load reductions in place of immediate blade maintenance.

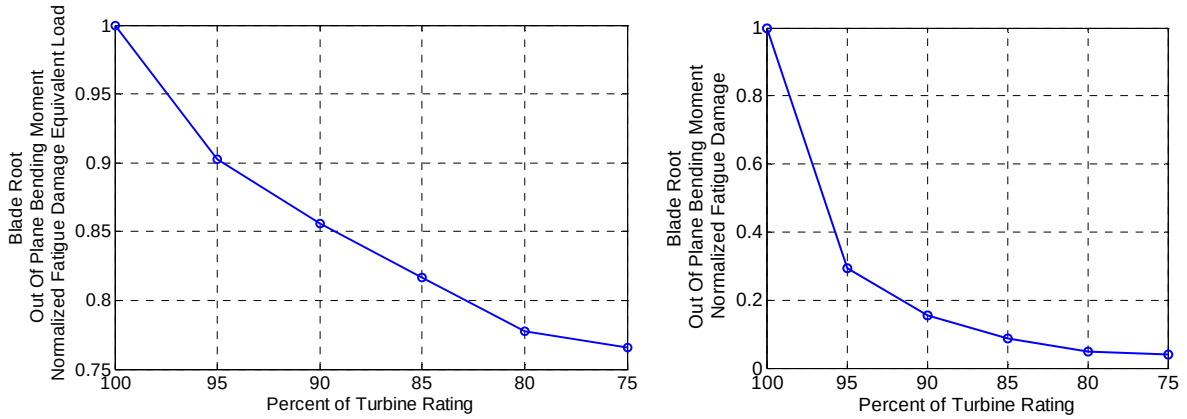


**Figure 43. Decrease in (a) normalized cyclic load amplitude and (b) normalized fatigue damage as a function of turbine rating; simulations performed in 11 m/s average wind speed.**

## 5.3. The Use of SHPM and Load Management for O&M

Many of the traditional analyses [7-12] of the benefits of SHPM systems into wind plant O&M take a passive view of the wind farm. This means that knowledge of the damage state of the turbine simply results in optimization of the maintenance of the turbines rather than changes in how the wind farm is operated. However, due to the difficulty of access associated with offshore wind turbines it may not always be desired, or possible, to repair a turbine as soon as a detectable amount of damage is present.

The decrease in loads and fatigue damage that can be achieved by derating a turbine (Section 5.2) demonstrates the feasibility of extending the life of a given turbine at the cost of a small percentage decrease in revenue. One of the benefits of this methodology is that for a single turbine even if maintenance cannot be performed when damage is detected, the turbine can be derated slightly so that it still generates revenue but does not accumulate large amounts of additional damage. This could potentially reduce the associated repair costs significantly if the transition between two different types of repairs can be avoided (see Section 5.1). A second benefit to the derating process that is especially relevant for offshore wind plants is that it this life extension methodology increases the possibility of servicing multiple turbines during a single visit to the offshore wind plant. Smart turbine load management, therefore enables the turbine operator to affect the progression of damage in a turbine so that the timing of operations and maintenance procedures can be optimized for the entire wind farm. Once quantitative damage size versus repair costs functions (Figure 39) have been determined, further simulations of an entire offshore wind plant could be used to quantitatively evaluate the cost reductions possible with a SHPM system and load management methodology.

# 6. CONCLUSIONS

This report provides an initial roadmap for integration of structural health and prognostics management (SHPM) into the O&M process for offshore wind plants. The key aspects of the work include (1) development of a multiscale modeling and simulation methodology to analyze the effects of damage in damaged operating turbines, (2) demonstration of this multiscale approach to perform sensitivity of damage studies for a candidate blade damage mechanism, (3) development of an initial conceptual damage and cost model for blade repair, and (4) identification and evaluation of smart turbine loads management (control) strategies based on SHPM for offshore wind plants.

A multiscale simulation methodology was developed for the investigation and development of SHPM methods for offshore wind turbine blades. The method relies on the propagation of damage from high fidelity component-level models to reduced order models that can be used in full turbine simulations so that the changes in the turbine's operational responses due to damage can be examined. These full turbine simulations can also be used to estimate the loads on individual components, such as turbine blades, and then be propagated back into to the high fidelity model to allow for further local analyses of the effects of damage to be conducted. By investigating the effects of damage on multiple scales, the developed methodology takes advantage of available software to investigate the underlying physical consequences of damage on both a local and global level. These simulations can then be used for many purposes including identification of global operational responses that are most sensitive to the damage (e.g. to evaluate sensing and detection options) and analysis of local effects of damage in the high-fidelity model (e.g. to estimate the remaining life or extent of the damage in the structure).

This report has demonstrated the application of the developed simulation-based methodology to perform a sensitivity of damage study of operational response measurements for the case of a TE (trailing edge) disbond on an offshore 5-MW wind turbine. A 61.5 meter blade model with a carbon fiber composite spar cap was developed using SNL's NuMAD software. The blade was then exported to ANSYS where the TE disbond was simulated by splitting the TE in half and constraining the bottom and top nodes to one another in the healthy portions of the blade. Reduced order models of the damaged blades were then created using SNL's BPE software. The analysis of these reduced order models demonstrated that the TE disbonds decreased the torsional stiffness of the blade around the disbond but did not significantly affect the blade's mass or stiffness in other directions. These reduced order blade models with varying levels of damage were included as part of a model of a 5-MW offshore turbine on a fixed monopole in 20 meters of water. The operational response of seven offshore turbine models with varying levels of damage was then simulated in both FAST and MSC.ADAMS. The operational responses were studied to quantify the sensitivity of the operational response to the TE disbonds. The sensitivities of the numerous operational responses (e.g. accelerations, moments) were quantified using measures that included analysis of statistical moments and standardized RMS difference. FAST simulations were found to be inadequate for modeling the effects of a TE disbond due to the fact that the torsional stiffness of the blades is not taken into account in FAST. However, from the ADAMS simulations it was apparent that the measurements which were the most sensitive to the presence and extent of the TE disbond were the pitching moments near the location of damage. The aerodynamic loads from the FAST simulations were calculated and

applied to the high fidelity ANSYS model, which also demonstrated that changes in the blade's strain field were localized around the edges of the disbond.

To examine how the structural health of each turbine could be used to optimize the operation and maintenance practices of an offshore wind plant, a qualitative damage size versus repair cost function for wind turbine blades was investigated. Additionally, smart load management (control) strategies were identified and simulations demonstrated that derating a turbine could be used to effectively decrease loads and significantly extend the fatigue life of a turbine while reducing the generated power by only a small percentage. The combination of the repair cost information along and the structural health of each turbine can be utilized in the optimization of damage mitigating control strategies to reduce the operations and maintenance costs associated with running an offshore wind energy plant.

# 7. FUTURE WORK

Rather than functioning as an in-depth investigation of all the possible areas of research in the SHPM of offshore wind turbines, this report has attempted to provide an initial "roadmap" into how the SHPM problem can be approached using a physics-based multiscale modeling and simulation methodology. As a consequence of this approach, there are a number of areas in which this initial report has only briefly touched on and are in need of further investigation.

In future work, this effort will be expanded to a more comprehensive system model in which the economics of power production and maintenance, sensitivity analyses of damages, and smart turbine load management (controls) will be analyzed to ensure the optimal operations strategy that balances maintenance processes with revenue production of the complete wind farm. This effort will consider cost-benefit trade-offs for traditional SCADA data streams as well as novel sensor or condition based monitoring system additions to traditional SCADA. In an additional avenue, SCADA data streams are likely to provide much more information than is the current practice because additional data mining and signal processing is possible.

Additional blade damage mechanisms in addition to TE disbond will be analyzed via similar sensitivity of damage studies to determine damage signatures that are potentially unique for different types of damage experienced in utility-scale wind turbine blades. The local analysis of the high-fidelity blade model will also include additional structural analyses beyond fatigue analysis. IEC standards for simulations will be used to establish critical damage sizes for these types of damage by determining the size of damage when the turbine no longer complies with certification requirements. A more complete model of the economics of integrating a SHPM system into offshore wind plants is required.

Another area that necessitates further investigation is the adequacy of the simple damage model used to model the TE disbond in this report. For example, the impact of the nonlinear surface contact in areas that have disbonds remains an area for future investigation. Such an exploration would include what effects the use of nonlinear contact constraints have on the equivalent stiffness values calculated by BPE, as well as the possible use of a nonlinear stiffness matrix in the damaged area in the full turbine simulations. The local strain sensitivity analysis should also be verified through a convergence analysis and ideally the model would be validated through the correlation with experimental strain measurements.

Based on the promising results from this study, another area that deserves further investigation is smart turbine loads management - the development of prognostic control and derating schemes. For example, results using Mode 2 and Mode 3 (as described in this report) or other more advanced derating schemes could be investigated and optimized. Furthermore, prognostic control algorithms that are based off mitigating damage growth or failures associated with the principal blade design drivers such as ultimate strength, deflection, and buckling should be investigated in addition to the fatigue analysis in this report.

Finally, the success of different damage detection algorithms for detecting various types and locations of damage remains future work. While this document focused solely on the use of time domain methods for the quantification of damage sensitivity, the developed multiscale

simulation methodology opens the doors for a wide variety of operational monitoring and damage detection methods to be investigated. However, as part of these investigations the influence of a wide amount of different parameters such as environmental changes and the impact of variable wind loadings would have to be investigated. Again, a more complete model of the economics of integrating a SHPM system into offshore wind plants is required along with evaluations of SHPM system performance.

These planned activities will provide a foundation for the future long-term research program aimed to support the needs of the offshore wind industry. The current activities can provide a starting point for moving from these FY11 simulation-based studies at Sandia to laboratory and field testing demonstration projects. Such testing can provide a deeper knowledge base regarding application and implementation of health monitoring to wind turbines, a database for evaluation of damage detection and sensing methods, and a means to evaluate how turbine-turbine interactions affect the methodologies.

# 8. REFERENCES


1. A.C. Levitt, W. Kempton, A.P. Smith, W. Musial and J. Firestone, "Pricing offshore wind power." *Energy Policy* (In Press) 2011.
2. W. Musial and B. Ram, *Large-Scale Offshore Wind Energy for the United State: Assessment of Opportunities and Barriers*, NREL Report No. TP-500-49229, Golden, CO, September 2010.
3. U.S. Department of Energy, *A National Offshore Wind Strategy: Creating an Offshore Wind Energy Industry in the United States,* Washington: Wind & Hydropower Technologies Program Report No. 5040, February 2011.
4. R. Wiser and M. Bolinger, *2010 Wind Technologies Market Report*, Lawrence Berkeley National Laboratory: Lawrence Berkeley National Laboratory. LBNL Paper LBNL-4820E, June 2011.
5. B. Snyder and M.J. Kaiser, "Ecological and economic cost-benefit analysis of offshore wind energy." *Renewable Energy* 34(6), pp. 1567-1578, 2009.
6. Y. Amirat, M.E.H Benbouzid, B. Bensaker, and R. Wamkeue, "Condition monitoring and fault diagnosis in wind energy conversion systems: a review." In *Proceedings 2007 IEEE International Electric Machines and Drives Conference*, Vol 2., pp. 1434-1439, 2007.
7. G. van Bussel, A.R. Henderson, C.A. Morgan, B. Smith, R. Barthelmie, K. Argyriadis, A. Arena, G. Niklasson, and E. Peltola, "State of the Art and Technology Trends for Offshore Wind Energy: Operation and Maintenance Issues," *Offshore Wind Energy EWEA Special Topic Conference*, Brussels, Belgium, December 2001.
8. L.W.M.M. Rademakers, H. Braam, M.B. Zaaiger, and G.J.W. van Bussel, "Assessment and optimisation of operation and maintenance of offshore wind turbines," in *Proceedings of the European Wind Energy Conference*, Madrid, Span, June 2003.
9. J. Nilsson and L. Bertling, "Maintenance management of wind power systems using condition monitoring systems – Life cycle cost analaysis for two case studies," *IEEE Transactions on Energy Conversion* 22(1), pp. 223-229, 2007.
10. C.C. Ciang, J.R. Lee, and H.J. Bang, "Structural health monitoring for a wind turbine system: a review of damage detection methods." *Measurement Science and Technology* 19(12), pp. 1-20, 2008.
11. F. Besnard, K. Fischer, and L. Bertling, "Reliability-centred asset maintenance – A step towards enhanced reliability availability and profitability of wind power plants" in *2010 IEEE PES Innovative Smart Grid Technologies Conference Europe (ISGT Europe)*, 2010.
12. Z. Hameed, S.H. Ahn, and Y.M. Cho, "Practical aspects of a condition monitoring system for a wind turbine with emphasis on its design, system architecture, testing and installation," *Renewable Energy*, 35(5), pp. 879-894, May 2010.
13. NWTC Design Codes (FAST by Jason Jonkman, Ph.D.). http://wind.nrel.gov/designcodes/simulators/fast/. Last modified 05-November-2010; accessed 05-November-2010.
14. R.R. Ryan, ADAMS – Multibody System Analysis Software, Multibody Systems Handbook. Berlin: Springer-Verlag, 1990.
15. J. Jonkman, S. Butterfield, W. Musial, and G. Scott, "Definition of a 5-MW Reference Wind Turbine for Offshore System Development," NREL/TP-500-38060, Golden, CO: National Renewable Energy Laboratory, February 2009.

16. Reference, MSU Database: MD-P2B; [±45/(0)4C]S; 55%vf; EP; Newport NB307; carbon prepreg; 85% Uni; 15% DB.
17. D.J. Malcolm and D.L. Laird, "Extraction of Equivalent Beam Properties from Blade Models." *Wind Energy*, 2007, 10, 135-137.
18. D.J. Malcolm and D.L. Laird, "Identification and Use of Blade Physical Properties," *AIAA 43rd Aerospace Sciences Meeting and Exhibit*, 2005.
19. D.J. Malcolm and D.L. Laird, "Modeling of Blades as Equivalent Beams for Aeroelastic Analysis," *AIAA 41st Aerospace Sciences Meeting and Exhibit*, 2003.
20. D.J. Malcolm and D.L. Laird, "Identification and Use of Blade Physical Properties," *AIAA 43rd Aerospace Sciences Meeting and Exhibit*, 2005
21. D.L. Laird, F.C. Montoya, and D. Malcolm, "Finite Element Modeling of Wind Turbine Blades." 43rd AIAA Aerospace Sciences Meeting and Exhibit, 2005, 9-17.
22. B. Resor, J. Paquette, D. Laird, and D.T. Griffith, "An Evaluation of Wind Turbine Blade Cross Section Analysis Techniques." 51st AIAA Structures, Structural Dynamics, and Materials Conference, 2010.
23. B. Resor and J. Paquette, "Uncertainties in Prediction of Wind Turbine Blade Flutter." 52nd AIAA/ ASME/ ASCE/ AHS/ ASC Structures, Structural Dynamics and Materials Conference, 2011.
24. Y. Chen and J.E. McInroy, "Estimation of Symmetric Positive-Definite Matrices from Imperfect Measurements," *IEEE Transactions on Automatic Control*, 47(10), pp. 1721-1725, 2002.
25. Jensen, F.M, "Failures in Trailing Edge Bondlines of Wind Turbine Blades," in *Proceedings of the 32nd Risoe International Symposium on Materials Science*, Roskilde, Denmark, 2011.
26. D.E. Adams, J.R. White, M. Rumsey, and C. Farrar, "Structural health monitoring of wind turbines: method and application to a HAWT," *Wind Energy*, 14(4), pp. 603-623, 2011.
27. M.A. Rumsey and J.A. Paquette, "Structural health monitoring of wind turbine blades, " in *Proceedings of SPIE Smart Structures and Materials & Nondestructive Evaluation and Health Monitoring,* San Diego, CA, March 2008.
28. A. Ghoshal, M.J. Sundaresan, M.J. Schulz, and P.F. Pai, "Structural health monitoring techniques for wind turbine blades," *Journal of Wind Engineering and Industrial Aerodynamics,* 85(3), pp. 309-324, 2000.
29. B.J. Jonkman and M.L. Buhl. *TurbSim user's guide [electronic resource]*. National Renewable Energy Laboratory, Golden, CO., 2006.
30. J. Bai and S. Ng, "Tests for Skewness, Kurtosis, and Normality for Time Series Data," *Journal of Business and Economic Statistics* 23(1), pp. 49-60, 2005.
31. C.R. Farrar and T.A. Duffey, "Vibration-Based Damage detection in Rotating Machinery." *Key Engineering Materials* Vols. 167-168, pp. 224-235, 1999.
32. J.R. White. "Operational Monitoring of Horizontal Axis Wind Turbines with Inertial Measurements," Doctoral Dissertation Purdue University (2010).
33. Z.I. Botev, J.F. Grotowski, and D.P. Kroese, "Kernel Density Estimation Via Diffusion." *The Annals of Statistics*, 38(5), pp. 2916-2957, 2010.
34. D. McMillan and G.W Ault, "Towards Quantification of Condition Monitoring benefit for Wind Turbine Generators," in *Proceedings European Wind Energy Conference*, Milan, pp. 112-116, May 2007.

35. D. McMillan and G.W. Ault, “Condition monitoring benefit for onshore wind turbines: sensitivity to operational parameters,” *IET Renewable Power Generation*, 2(1), pp. 60-72, March 2008.
36. NWTC Design Codes (Crunch by Marshall Buhl) Last modified 01-April-2008; accessed 01-April-2008.

## Distribution:

Cecelia Sterling (5)
Office of Wind and Hydropower Technologies
EE-2B Forrestal Building, U.S. DOE
1000 Independence Ave. SW
Washington, DC 20585

Library (5) NWTC
NREL/NWTC
1617 Cole Boulevard
Golden, CO 80401

## Internal Distribution

MS 1124 D.T. Griffith, 6122 (10)
MS 1124 Wind Library, 6121 (10)
MS 0899 RIM-Reports Management, 9532 (electronic copy)


Sandia National Laboratories